

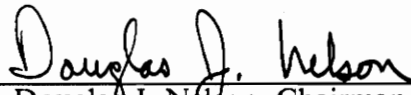
# THERMAL MODELING OF HYBRID MICROELECTRONICS

by

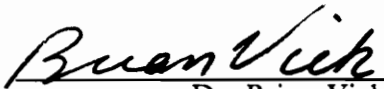
Herbert H. Eades, III

Thesis submitted to the Faculty of the  
Virginia Polytechnic Institute and State University  
in partial fulfillment of the requirements for the degree of  
Master of Science  
in  
Mechanical Engineering

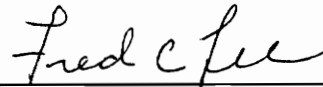
APPROVED:



Dr. Douglas J. Nelson, Chairman



Dr. Brian Vick



Dr. Fred C. Lee

July, 1990

Blacksburg, Virginia

C.2

LD  
5655  
V855  
1990  
E323  
C.2

# **THERMAL MODELING OF HYBRID MICROELECTRONICS**

by

Herbert H. Eades, III

Dr. Douglas J. Nelson, Chairman

Mechanical Engineering

(ABSTRACT)

As the size of hybrid microelectronics is reduced, the power density increases and thermal interaction between heat-producing devices becomes significant. A nondimensional model is developed to investigate the effects of heat source interaction on a substrate. The results predict the maximum temperature created by a device for a wide range of device sizes, substrate thicknesses, device spacings, and external boundary conditions. They can be used to assess thermal interaction for preliminary design and layout of power devices on hybrid substrates.

Previous work in this area typically deals with semi-infinite regions or finite regions with isothermal bases. In the present work, the substrate and all heat dissipating mechanisms below the substrate are modeled as two separate thermal resistances in series. The thermal resistance at the base of the substrate includes the bond to the heat sink, the heat sink, and convection to a cooling medium. Results show that including this external resistance in the model can significantly alter the heat flow path through the substrate and the spreading resistance of the substrate. Results also show an optimal thickness exists to minimize temperature rise when the Biot number is small and the device spacing is large.

Tables are presented which list nondimensional values for maximum temperature and spreading resistance over a wide range of substrate geometries, device sizes, and boundary conditions. A design example is included to demonstrate an application of the results to a practical problem. The design example also shows the error that can result from assuming an isothermal boundary at the bottom of the substrate rather than a finite thermal resistance below the substrate.

Several other models are developed and compared with the axisymmetric model. A one-dimensional model and two two-dimensional models are simpler than the axisymmetric model but prove to be inaccurate. The axisymmetric model is then compared with a full three-dimensional model for accuracy. The model proves to be accurate when sources are symmetrically spaced and when sources are asymmetrical under certain conditions. However, when the sources are asymmetrical the axisymmetric model does not always predict accurate results.

# Dedication

This work is dedicated to my parents, Mr. and Mrs. Herbert H. Eades Jr., for their love and support through all of my endeavors.

## Acknowledgements

Many thanks to my advisor, Dr. Douglas J. Nelson, whose guidance and support have been invaluable. Without you, I doubt that I would have ever attempted this work. I would also like to thank my committee members, Dr. Brian Vick and Dr. Fred C. Lee, for their time and efforts, and the Virginia Power Electronics Center for the support of this work.

To my parents, my sister, Diane Schnupp, and my other family members. Your love and encouragement have given me motivation to succeed in all of my endeavors. Your pride in me has been more gratifying than any other acknowledgement of success. I love you very much.

Special thanks to Karen Steinbach (L.M.) for her support and understanding throughout the past year.

# Table of Contents

<b>1.0</b>	<b>Introduction</b>	<b>1</b>
<b>1.1</b>	<b>Modeling Techniques</b>	<b>9</b>
<b>2.0</b>	<b>Literature Review</b>	<b>12</b>
<b>3.0</b>	<b>One-Dimensional Modeling</b>	<b>20</b>
<b>4.0</b>	<b>Two-Dimensional Modeling</b>	<b>26</b>
<b>4.1</b>	<b>Slice Model</b>	<b>29</b>
<b>4.2</b>	<b>Slab Model</b>	<b>35</b>
<b>4.3</b>	<b>Results</b>	<b>37</b>
<b>5.0</b>	<b>Axisymmetric Modeling</b>	<b>42</b>
<b>5.1</b>	<b>Dimensional Model</b>	<b>43</b>
<b>5.2</b>	<b>Nondimensionalization</b>	<b>48</b>

<b>6.0 Results of Axisymmetric Modeling</b>	<b>55</b>
6.1 Effects of the Biot Number	58
6.2 Effects of the Nondimensional Thickness	61
6.3 Effects of the Nondimensional Width	64
6.4 Trends in the Results	64
 <b>7.0 Design Example</b>	 <b>66</b>
7.1 Maximum Temperature Calculation	67
7.2 Isothermal Boundary Assumption Error	68
 <b>8.0 Verification of Results</b>	 <b>71</b>
8.1 Three-Dimensional Modeling	71
8.2 Experimentation	78
 <b>9.0 Conclusions and Recommendations</b>	 <b>85</b>
9.1 Conclusions	85
9.2 Recommendations	89
 <b>List of References</b>	 <b>91</b>
 <b>Appendix A. Design Example Calculations</b>	 <b>93</b>
A.1 Maximum Temperature Calculation	96
A.2 Isothermal Boundary Assumption Error	96
 <b>Vita</b>	 <b>99</b>



## List of Illustrations

Figure 1. Schematic drawing of a hybrid power supply	2
Figure 2. One-dimensional model of one device on a substrate	4
Figure 3. Two-dimensional "slice" model	5
Figure 4. Two-dimensional "slab" model	6
Figure 5. Dimensional axisymmetric model	8
Figure 6. Spreading angle of heat propagation	21
Figure 7. Area and magnitude of heat flux	22
Figure 8. Slice model used in HEAT	27
Figure 9. Slab model used in TASS	28
Figure 10. Tolerance values in HEAT	32
Figure 11. Symmetrically spaced heat sources on a substrate and heat sink	45
Figure 12. Axisymmetric approximation of one source on a substrate	47
Figure 13. Dimensional axisymmetric model	49
Figure 14. Nondimensional axisymmetric model	51
Figure 15. Equivalent thermal network of the axisymmetric model	53
Figure 16. Heat flux through a substrate for a large Biot number	59
Figure 17. Heat flux through a substrate for a small Biot number	60
Figure 18. Nondimensional temperature increase at small thicknesses	62
Figure 19. Nondimensional spreading resistance increase at small thicknesses	63

Figure 20. Maximum temperature examples for practical and isothermal boundary conditions ..... 69

Figure 21. TAMS model of two sources placed eccentrically ..... 75

Figure 22. Axisymmetric model of one source with reduced substrate area to compensate for eccentrically placed sources ..... 76

Figure 23. Image of a resistor and its leads produced by a thermal imaging system 84

# List of Tables

Table 1. Accuracy of one-dimensional results vs. axisymmetric model results . . . .	25
Table 2. Comparison of grids to estimate discretization error . . . . .	30
Table 3. Comparison of Biot number to temperature difference ratio . . . . .	34
Table 4. Comparison of grids in TASS to estimate discretization error . . . . .	36
Table 5. Accuracy of HEAT results vs. axisymmetric model results . . . . .	38
Table 6. Accuracy of TASS results vs. axisymmetric model results, $B = 4$ . . . . .	39
Table 7. Accuracy of TASS results vs. axisymmetric model results, $B = 20$ . . . . .	40
Table 8. Nondimensional maximum temperatures . . . . .	56
Table 9. Nondimensional spreading resistances . . . . .	57
Table 10. Axisymmetric results vs. TAMS as two sources become asymmetric on a large substrate . . . . .	73
Table 11. Axisymmetric results vs. TAMS as two sources become asymmetric on a small substrate . . . . .	74
Table 12. Experimental results for temperatures created by one device placed symmetrically on a substrate . . . . .	81
Table 13. Comparison of TAMS results to experimental results . . . . .	82

## Nomenclature

<b>A</b>	nondimensional substrate thickness = $\frac{t}{d}$ or area (m <sup>2</sup> )
<b>b</b>	equivalent diameter of substrate in dimensional model (m)
<b>B</b>	nondimensional substrate diameter = $\frac{b}{d}$
<b>Bi</b>	Biot number = $\frac{ht}{k}$
<b>d</b>	equivalent diameter of heat source in dimensional model (m)
<b>D</b>	nondimensional heat source diameter = 1.0
<b>h</b>	convective heat transfer coefficient (W/m <sup>2</sup> -K)
<b>k</b>	thermal conductivity of the substrate (W/m-K)
<b>K</b>	nondimensional thermal conductivity of the substrate = 1.0

<b>q</b>	heat produced by the heat source (W)
<b>Q</b>	nondimensional heat produced by the source
<b>r</b>	radial coordinate (m)
<b>R</b>	nondimensional radial coordinate or thermal resistance (K/W)
<b>t</b>	substrate thickness (m)
<b>T</b>	temperature (K)
<b>z</b>	depth coordinate (m)

### ***Greek Letters***

<b><math>\theta</math></b>	nondimensional temperature variable = $\frac{T - T_0}{q_d'' d/k}$
<b><math>\Phi</math></b>	nondimensional resistance variable = $k\sqrt{A_d} R$

### ***Subscripts***

<b>0</b>	ambient
<b>b</b>	equivalent diameter of the substrate

<b>d</b>	equivalent diameter of the heat source
<b>ext</b>	quantity external to the substrate
<b>hs</b>	heat sink
<b>max</b>	maximum quantity
<b>S1</b>	quantity at the top surface of the substrate
<b>S2</b>	quantity at the bottom surface of the substrate
<b>sp</b>	spread
<b>sub</b>	substrate
<b>tot</b>	total

***Superscripts***

<b>-</b>	mean or average
<b>"</b>	per unit area

# 1.0 Introduction

The physical problem described in this thesis is a hybrid power supply. A rectangular substrate has a circuitry design, containing several devices, such as switching transistors, rectifier diodes, resistors, etc., on its top face. These devices generate heat as they operate. Below the substrate is a heat sink, typically made of aluminum for high thermal conductivity, and possibly fins or other mechanisms to aid dissipation of heat to the ultimate heat sink, which is usually air. The devices are connected to the substrate with some type of die attach, and the substrate is bonded to the heat sink, usually with an epoxy. Figure 1 displays a schematic drawing of several devices on a substrate attached to a finned heat sink. When several devices are placed on a hybrid substrate, they interact thermally. As power density increases, the thermal interaction and junction temperatures increase. This temperature rise can adversely effect performance and reliability of the device.

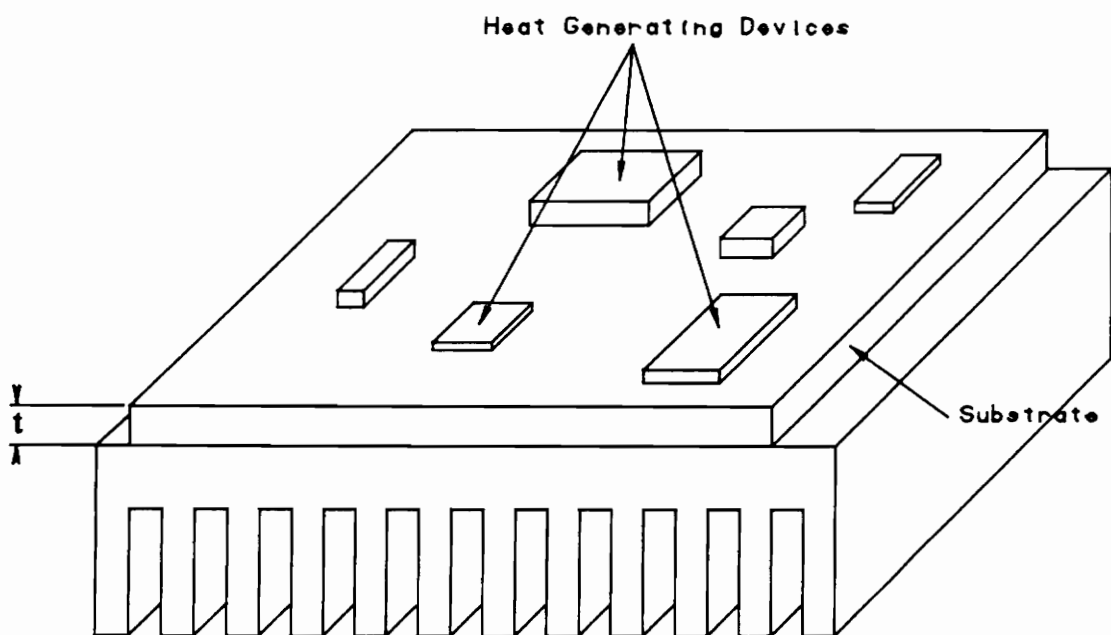


**Figure 1. Schematic drawing of a hybrid power supply**



Several models have been developed to investigate the effects of substrate design on temperature rise. Preliminary models include a one-dimensional model and two two-dimensional models. An axisymmetric model was then developed and its accuracy was verified with a full three-dimensional model. The results predict the maximum temperature of the device for a spectrum of geometries and boundary conditions. They can be applied to practical design of hybrid power supplies to analyze thermal interaction.

A one-dimensional model computes the maximum temperature created by a heat source on a substrate without interaction between heat sources. The area of heat transfer through the substrate increases as the heat propagates downward through the substrate by allowing the heat to flow outward at a constant spread angle. The exact value is not known and changes depending on boundary conditions and substrate material. However, it is often assumed to be forty-five degrees, corresponding to a semi-infinite medium. A one-dimensional model of one device on a substrate is shown in Fig. 2.

Two two-dimensional models analyze a substrate with symmetrical heat sources. A cross-sectional, or slice, model, shown in Fig. 3, examines the temperature variation through the thickness of the substrate with varying values of resistance to heat flow below the substrate. This resistance is modeled as an equivalent thermal convective coefficient,  $h_{eq}$ , in both two-dimensional models. A slab model, shown in Fig. 4, assumes the temperature gradient through the thickness of the substrate is small. Steady-state temperatures over the substrate surface are then calculated.

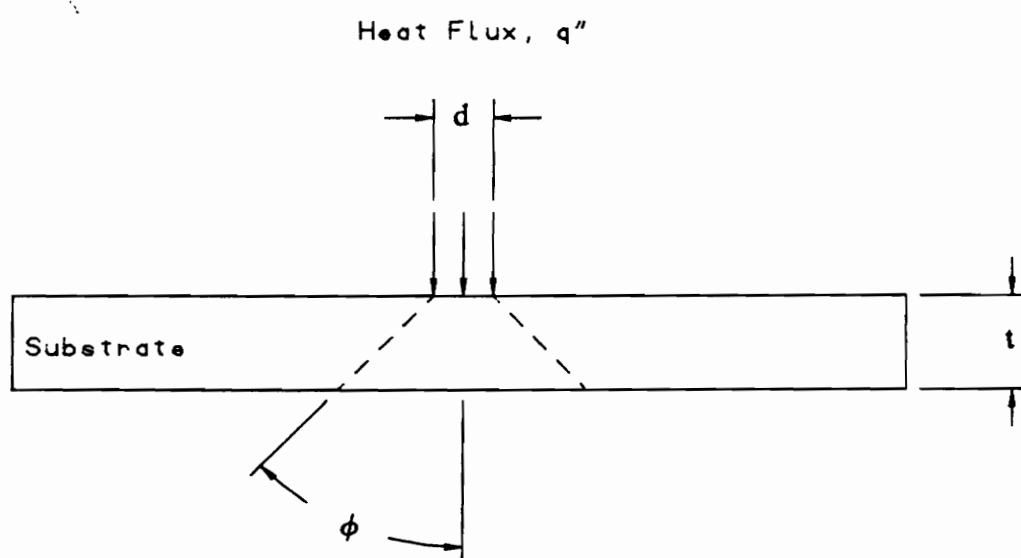


Figure 2. One-dimensional model of one device on a substrate

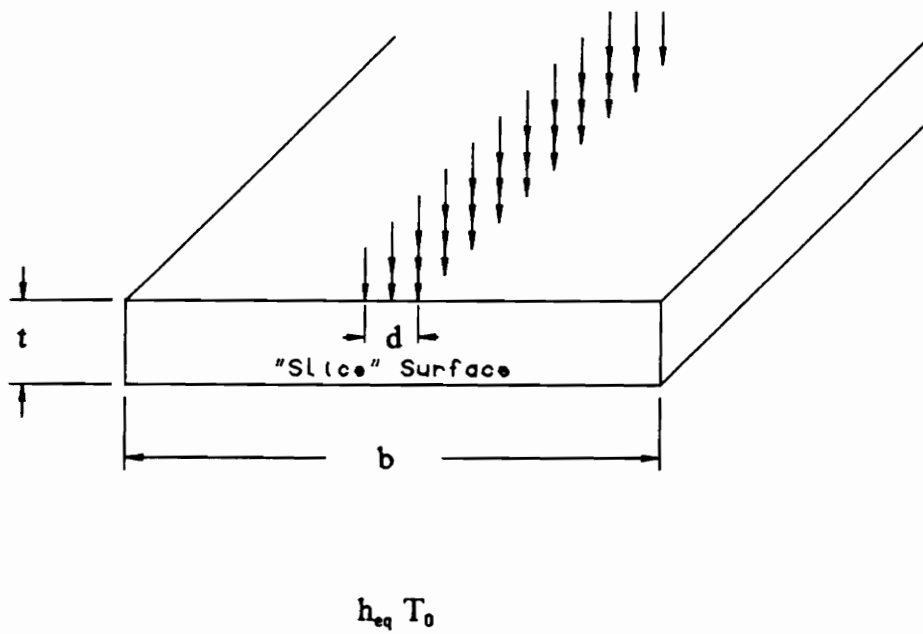


Figure 3. Two-dimensional "slice" model

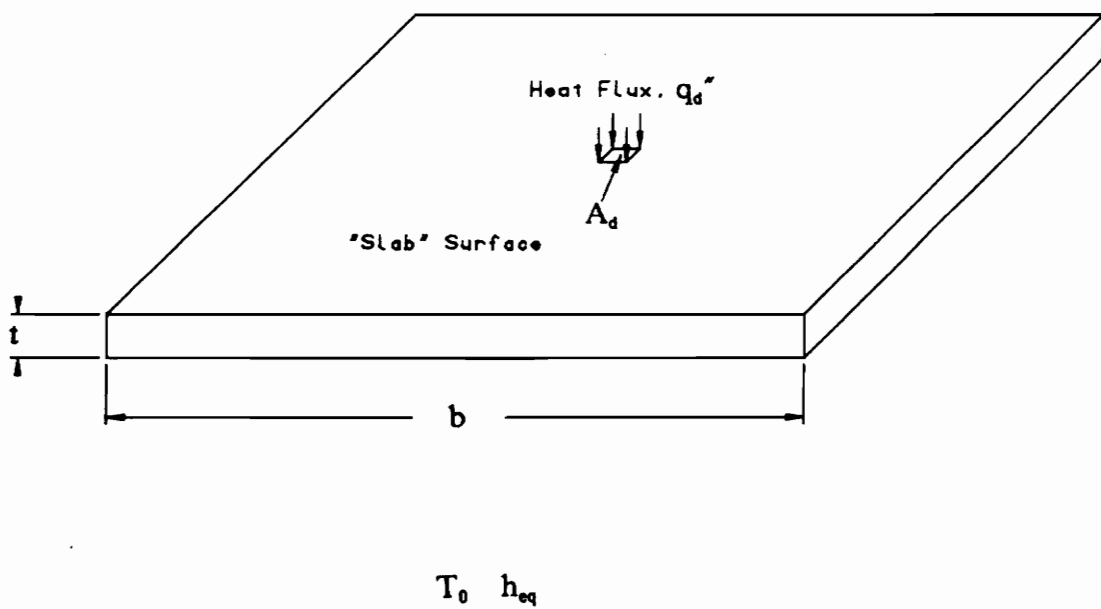


Figure 4. Two-dimensional "slab" model

An axisymmetric model divides the problem into a series of two resistances: the resistance of the substrate and the resistance of everything external to the substrate. This external resistance includes the resistance of the bond to the heat sink, the heat sink, and convection from the heat sink to air, and is modeled as an equivalent convective coefficient. Figure 5 shows the axisymmetric model with dimensional parameters. The model is nondimensionalized, reducing the number of parameters to three. The thickness and width of the the substrate may be independently varied from very thin and narrow to semi-infinite. The Biot number, which incorporates the external resistance below the substrate, allows for a wide variety of boundary conditions below the substrate. The spreading resistance through the substrate is calculated from a two-dimensional axisymmetric finite element solution for the temperature distribution through the substrate. The results are valid for a general substrate conductivity, allowing comparison between different substrate materials such as alumina and aluminum nitride.

A three-dimensional analysis was performed using TAMS (Ellison, 1978). This program yields a Fourier series solution for a multi-layered system with lumped parameter thermal resistances on both the top and bottom surfaces. Each resistance terminates away from the substrate at a unique sink temperature. In addition to this, temperatures were experimentally measured using an infrared thermal imaging system. Results of the axisymmetric and experimental models are compared to the three-dimensional results for accuracy.

Several papers dealing with topics such as spreading angles and thermal interaction of devices have previously been published. However, assumptions are made in these mod-

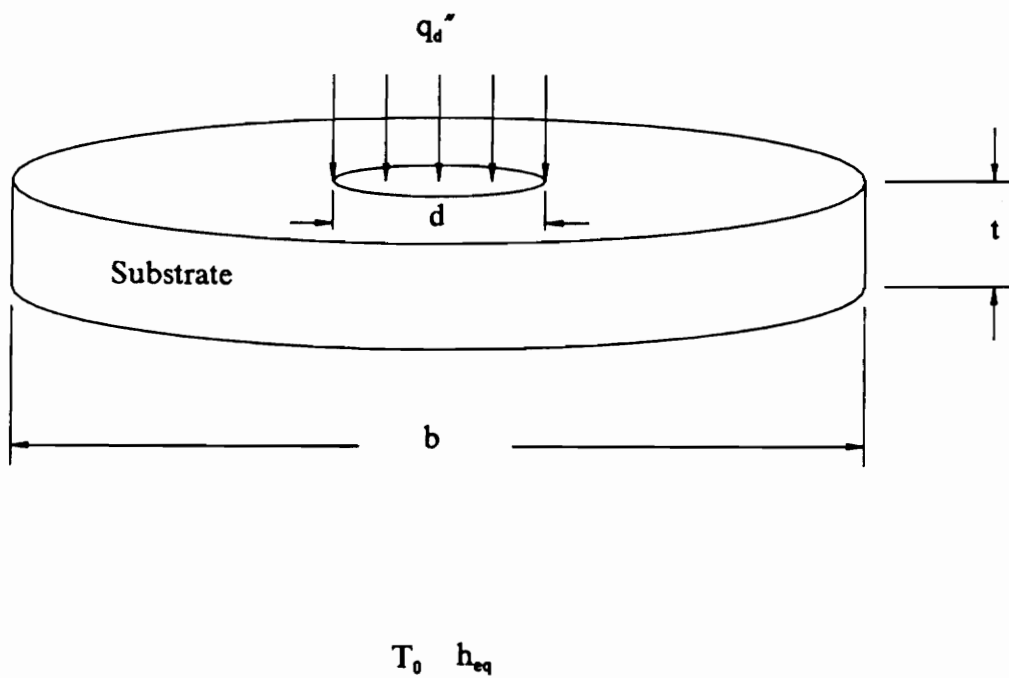


Figure 5. Dimensional axisymmetric model

els which may influence the accuracy of the results when applied to hybrid substrates. In the present work, the geometry is modeled as a finite layer, similar to an actual substrate, rather than as a semi-infinite region. Also, boundary conditions allow a finite resistance of variable magnitude below the substrate rather than assuming a constant temperature along the bottom of the substrate.

The results of this work predict maximum temperatures created by a device on a substrate or by several symmetrically spaced devices interacting on a substrate. They also predict the resistance to heat transfer through the substrate. Several parameters are varied over a wide range of practical values. They include the Biot number and the width and thickness of the substrate relative to the size of the heat source. Thus, a wide range of geometries and boundary conditions are considered. The results are tabulated and presented in this work.

## ***1.1 Modeling Techniques***

Several methods are used to model the physical problem described above. The simplest model that provides accurate temperature values is desired. Therefore, many different models are presented in this thesis. The three-dimensional model described in Chapter 8 is assumed to be accurate, and the axisymmetric model is compared to it for accuracy. Because the axisymmetric model proves to be accurate when heat sources are symmetrically spaced, the other models are compared to it for accuracy. In order to create

similar models for comparison, the one-dimensional and two-dimensional models are converted to nondimensional axisymmetric form, like the axisymmetric model, and described in terms of several nondimensional variables. The purpose of this section is to describe some terms which are used in nondimensionalizing the models and the procedure for comparing models.

For purposes of comparison, all of the models are converted into nondimensional form. This reduces the number of variables to three. An equivalent diameter of the source,  $d$ , is defined as a length scale. It is found by converting the heat source area to a circular region, holding the area constant, and using the diameter of this circle. The thickness of the substrate,  $t$ , and the width of the substrate,  $b$ , are nondimensionalized by dividing their value by  $d$ . Like the heat source area,  $B$  represents an equivalent diameter of substrate. Its area is defined by symmetry between surrounding sources and the boundary of the substrate.

The third nondimensional parameter is the Biot number,  $Bi$ . It is defined as the thermal resistance to heat transfer through the substrate divided by the thermal resistance to heat transfer below the substrate. This ratio reduces to the formula  $\frac{ht}{k}$ , where  $h$  is an equivalent convective heat transfer coefficient representing all heat dissipating mechanisms below the substrate,  $t$  is the thickness of the substrate, and  $k$  is the thermal conductivity of the substrate.

Nondimensional results from the axisymmetric model for the maximum temperature created by a heat source,  $\theta$ , are tabulated in Chapter 6. When the one-dimensional and



two-dimensional models are converted into nondimensional parameters,  $A$ ,  $B$ , and  $Bi$ , accurate maximum temperature values may be obtained from the results of the axisymmetric modeling using the table in Chapter 6. This temperature is compared with the maximum temperature predicted by a model to determine the accuracy of the model.

The next chapter describes some of the literature reviewed and its contribution to this work. The subsequent chapters describe the one-dimensional model, the two two-dimensional models, and the axisymmetric model in depth. Results of the axisymmetric model are then presented and discussed, followed by a design example analyzed using the axisymmetric results. The example also describes the error caused by assuming that the bottom of the substrate is isothermal instead of adding a finite resistance to the bottom of the substrate. The next chapter presents the three-dimensional model and experimental results used to verify the axisymmetric results. Finally, conclusions are drawn and recommendations for further study are made.

## 2.0 Literature Review

As a foundation to studying the thermal modeling of hybrid circuits, a review of relevant literature was undertaken. Different modeling methods and different geometries considered were of particular interest, along with one-dimensional spreading angle models. Some of the methods used to analyze electrical components found in the literature are the Fourier transform method and the finite element method. Some of the different geometries analyzed in the literature include a trimming cut in screen printed resistors, complex multi-material power chip base combinations, and a semiconductor die. Two articles describe the testing of a spreading angle through a substrate. However, few papers consider the interaction of more than one heat source or the maximum temperatures produced by this interaction.

A one-dimensional heat spreading angle is analyzed by David (1977). The heat spread model for thermally conductive paths less than twice the die dimension produces a

spread angle of  $26.6^\circ$ . This angle was determined from a best-fit curve of data points obtained from a three-dimensional model. One drawback of this method is that a constant temperature at the bottom of the hybrid package is assumed. Frey and Kane (1985) estimate the heat spreading angle to be constant. As the material thickness goes to infinity, the angle is approximately  $45^\circ$ . For lower values of thickness, the angle is said to decrease, with the heat spreading down more than out along the plane of the substrate.

A review of thermal contact resistance as applied to microelectronic equipment is presented by Antonetti and Yovanovich (1984). Although contact resistances are not considered in this work, Antonetti and Yovanovich summarize methods of determining spreading resistance in microelectronic packages. They define the spreading, or constriction, resistance as the temperature difference between the average junction temperature and some reference temperature, divided by the total heat flow rate from the junction. The chip is assumed to be a semi-infinite body because it is large compared to the junction size. When the spacing between adjacent junctions becomes comparable to the characteristic dimension of the junction area, Antonetti and Yovanovich reduce the semi-infinite region to an adiabatic circular cylinder of radius equal to one-half the junction spacing, called a flux tube.

Negus et al. (1989) consider a similar constriction resistance based on the area of contact of the heat source on a body. They nondimensionalize this resistance by multiplying it by the thermal conductivity of the body and a characteristic length. It is determined that using the square root of the source contact area as the characteristic length gives similar

results for many different geometries. The present work utilizes this nondimensionalization technique to define a spreading resistance through the substrate, an external resistance below the substrate, and a total resistance.

Several papers compare higher dimensional models with lower dimensional models for accuracy and complexity. For example, Fast et al. (1987) relate the effects of several parameters, such as thermal conductivity, geometry, and fluid velocity, to source temperature in comparing one- and two-dimensional models. This analysis is applied to microelectronic printed circuit boards. One heat source is placed on the surface of the PCB and the models are nondimensionalized and correlated against several dimensionless groups. The two-dimensional model is solved from Laplace's equation using a boundary integral method technique. Both models are solved for a range of thermal conductivity, fluid velocity, source heat flux, and board thickness. A two-dimensional correlation is presented for a single source on a flat plate. However, the maximum Biot number is 3.8, making the correlation valid for small Biot numbers only.

The results of a three-dimensional finite element thermal analysis of a chip and spreader are compared with those obtained from a two-dimensional axisymmetric approximation and presented in an article by Kadambi and Abuaf (1983). Numerical solutions to all the three-dimensional problems are obtained by using a computer program. The solution of the axisymmetric problem is done using a two-dimensional finite element program. The results of the numerical calculations are also confirmed by an approximate analytical solution obtained by using an integral method. The axisymmetric approximation of a silicon chip and copper base is done by keeping the areas of the chip and

base constant. The author's work supports the use of an axisymmetric approximation of a three-dimensional model in the present work.

Rottiers and May (1988) compare two- and three-dimensional models to investigate the hot spot effect occurring at the termination point of a trimming cut in screen printed resistors. Two-dimensional models, solved using the boundary element method and a Fourier expansion, and three-dimensional models, solved by Fourier series, are analyzed for steady-state and transient response. The two-dimensional results agree very well with the exact three-dimensional analysis outside the vicinity of the hot spot. Therefore, temperatures are calculated two-dimensionally across the whole substrate and "zooming" is done around a hot spot, where a three-dimensional equation is then solved in a limited volume.

The determination of the thermal resistance of complex multi-material power chip base combinations for steady state and transient conditions is determined by Kadambi and Abuaf (1985). In a two-dimensional analysis of the three-dimensional geometry, two perpendicular cuts were analyzed using a thermal analysis computer program. In the three-dimensional analysis, a finite element analysis package was used. It was found that three-dimensional problems can be approximated by one axisymmetric and two two-dimensional models. The axisymmetric model predicts the maximum chip temperatures, while the two two-dimensional models provide temperature distributions along two orthogonal cross-sections.

Several methods are used to solve two-dimensional models of a heat source on a substrate. The problems in the evaluation of temperature distribution of hybrid integrated circuit substrates are discussed by Wehrhahn (1985). A two-dimensional model is described which neglects any temperature difference through the thickness of the substrate. The Poisson equation with Neumann boundary conditions describes the model. It is solved using the Fourier transform method. Wehrhahn concludes that the thermal conductivity of the substrate has a large influence on temperature distribution through the substrate.

Two two-dimensional models are presented by Ferraris and Tudanca (1979) which analyze the heat conduction problem in hybrid circuits for two different geometries. The thickness of the substrates is considered negligible because they are very thin and have relatively high thermal conductivities. Circular shaped substrates with centered circular resistive films and rectangular shaped substrates with central rectangular resistive films are analyzed for maximum temperatures by solving the heat conduction equation with the appropriate boundary conditions.

Kennedy (1960) develops an analytical solution for temperature distribution from a uniform heat flux acting upon a finite circular cylinder. Though he only considers boundary conditions of isothermal and insulated, the geometry of the cylinder varies over a fairly wide spectrum. The present work advances Kennedy's ideas to include a wider variation of geometry and additional kinds of boundary conditions.

A series solution for the local surface temperature history of a semi-infinite body heated over a circular region is presented by Beck (1980). Inside this region the heat flux is constant while the surface outside the region is insulated. A solution is also presented for certain interior locations at "large" times.

The accuracy of two-dimensional models is often measured by comparison with three-dimensional models. In the present work, axisymmetric results are compared with three-dimensional results obtained using a computer program entitled TAMS. TAMS analyzes multi-layer microelectronic devices, as described in a paper by Ellison (1978) and also in a book by Ellison (1984). The program computes the maximum temperature of multiple sources with, if required, anisotropic thermal conductivity in up to four layers. Convective coefficients are input to allow variable resistances above and below the substrate. Sources may be at the surface of the structure or buried between layers. The three-dimensional solution provided is a Fourier series with up to seventy terms. A convergence check is also provided.

Using another three-dimensional analysis, Negus and Yovanovich (1987) discuss the development of a thermal analysis procedure for a semiconductor die with interacting heat sources. The procedure was carried out by solving the full three-dimensional governing partial differential equations and boundary conditions within the die. Results show a mathematical solution for temperature distribution throughout a die. However, since isothermal conditions are assumed along the bottom of the substrate, results from the present work are not compared to Negus' and Yovanovich's results.

Jensen et al. (1987) investigate the relative importance of materials improvements versus design factors in thermal management of microelectronics packages. The authors develop a three-dimensional model of one device on a substrate solved using the finite element method for temperatures. They conclude that for packages dependent upon cooling by natural or forced convection in-plane improvements in thermal conductivity of the substrate are more critical than out-of-plane improvements since a high in-plane conductivity allows the heat to spread over a greater surface area. The authors also conclude that out-of-plane improvements in thermal conductivity of the substrate are much more important when a heat sink is in contact with the bottom of the substrate. However, an isothermal boundary at the bottom of the substrate is assumed when a heat sink is in contact with the bottom of the substrate.

Some experimental techniques for measuring temperatures on a substrate were examined. In the same paper that is described above, Ferraris and Tudanca (1979) experimentally measure the film temperatures with an infrared pyrometer at the hottest point. Temperature measurements are taken with the substrate mounted vertically and horizontally and values of the convection coefficient are presented. This coefficient is slightly larger for substrates mounted vertically due to natural convection. Correlations are presented to calculate the convection coefficient based on the area of the substrate.

A test configuration is described by DeMey and Demolder (1987) which allows a comparison between experimental results and a theoretical thermal analysis. Temperatures are measured using a Probye thermographic camera on a blackened substrate, which is used to obtain a uniform infrared emissivity. By comparing experimental data with an



analytical solution, the convection coefficient and thermal conductivity of the substrate are calculated. A similar procedure is used on a transient model to determine a value for the volumetric heat capacity.

None of the literature reviewed discusses the interaction of two heat sources on a substrate. However, the information found provides several effective methods of two- and three-dimensional analysis. Also, heat spreading angles different from the standard value of  $45^\circ$  are found in the literature. A heat spreading angle is used in a one-dimensional approximation using thermal resistances. Thus, the literature review not only verifies the uniqueness of the project, but also provides useful information for it.

### 3.0 One-Dimensional Modeling

A one-dimensional model can be used to compute the maximum temperature created by a heat source on a substrate without interaction between heat sources. The area of heat transfer through the substrate increases as the heat propagates downward through the substrate. This is modeled by considering a heat spreading angle, with the angle of heat propagation,  $\phi$ , shown in Fig. 6. The exact value is not known and changes depending on boundary conditions and substrate material. However, it is approximated to be  $45^\circ$ . Several one-dimensional models are compared to axisymmetric models for accuracy.

To model the system, a uniform heat flux is applied to a substrate, as shown in Fig. 7. The resistances through the substrate and below the substrate for practical substrate dimensions are calculated, and the temperature of the atmosphere is set as a constant value. From this data, the temperature at the top of the substrate is found. Three ge-

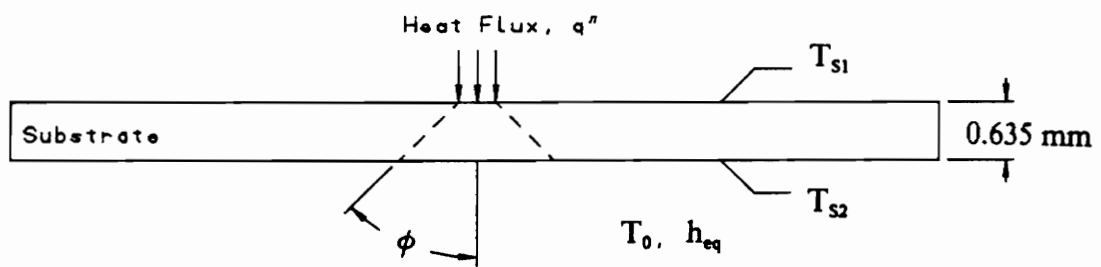
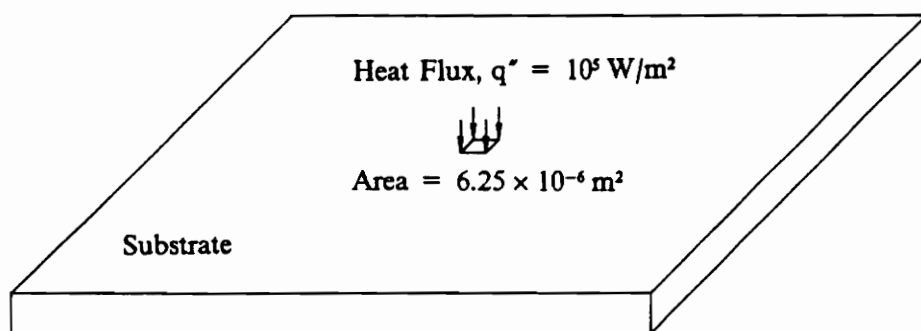


Figure 6. Spreading angle of heat propagation



**Figure 7. Area and magnitude of heat flux**

ometries are considered:  $A = 0.1, 0.5$  and  $1.0$ . At each geometry, five Biot numbers are considered:  $0.01, 0.1, 1.0, 100.0$  and infinity. These geometries and boundary conditions are used to incorporate all practical situations.

Each model is solved for a value of total resistance to heat transfer through the substrate and heat sink to ambient conditions. By presenting the total resistance, numerical values become independent of the heat source strength. The maximum temperature rise created by a source can be calculated by multiplying total resistance by source strength.

Two-dimensional axisymmetric results are presented later in this work. To compare one-dimensional results with the axisymmetric results, the thickness of the substrate,  $A$ , and the Biot number are varied, as described above. For each thickness, the area of heat transfer through the substrate, according to the spreading angle concept, was calculated at the middle and at the bottom of the substrate. The total resistance was then calculated by adding the resistance to conduction through the substrate,  $\frac{t}{kA}$ , where average the area,  $A$ , is measured at the middle of the substrate, to the resistance below the substrate,  $\frac{1}{hA}$ , where the area for heat loss,  $A$ , is measured at the bottom of the substrate. The convective heat transfer coefficient used is an equivalent term based on the Biot number. The area at the bottom of the substrate is converted into a nondimensional substrate width parameter,  $B$ . From axisymmetric results, the  $B$  closest to, but greater than, this value is used for comparison.

When one-dimensional results with a constant heat spreading angle of  $45^\circ$  are compared to the axisymmetric results, the one-dimensional results generally are not very accurate,

as shown in Table 1. However, under certain conditons one-dimensional models are extremely accurate. For example, when  $A = 0.1$  and  $Bi = 0.1$ , the error is only +7.01%. The positive sign on error indicates that the one-dimensional model yields conservative values. In other words, the one-dimensional maximum temperature is higher than that predicted by axisymmetric results. Table 1 shows that for each geometry considered, the error is positive at small Biot numbers and becomes negative at larger Biot numbers. Therefore, at each geometry there exists some Biot number where the one-dimensional model matches axisymmetric results exactly. The problem, however, is that the Biot number which provides exact results is unknown unless results are compared to axisymmetric values. Of course, if axisymmetric values are known a one-dimensional model is unnecessary.

One-dimensional models are simple, easy to understand, and provide a fast method of predicting maximum temperatures on a substrate using only a calculator. However, problems arise in deciding what heat spreading angle to use. Also, results are generally inaccurate. For Biot numbers of 0.1 and greater, results are within about forty percent of the axisymmetric results using a  $45^\circ$  heat spreading angle. Therefore, one-dimensional models are generally not very accurate but can provide an approximate temperature rise quickly and easily.

Table 1. Accuracy of one-dimensional results vs. axisymmetric model results

Bi	A = 0.1			A = 0.5			A = 1.0		
	$R_{tot,1D}$ (K/W)		$R_{tot,AXI}$ (K/W)	$R_{tot,1D}$ (K/W)		$R_{tot,AXI}$ (K/W)	$R_{tot,1D}$ (K/W)		$R_{tot,AXI}$ (K/W)
			% Error			% Error			% Error
0.01	281.8	174.3	+ 61.7	510.2	363.3	+ 40.4	455.6	268.0	+ 70.0
0.1	31.16	29.12	+ 7.01	59.04	49.97	+ 18.2	54.59	42.40	+ 28.8
1.0	6.099	7.759	-21.4	13.93	18.10	-23.0	14.48	19.65	-26.3
100.0	3.342	4.046	-17.4	8.962	13.71	-34.6	10.07	16.76	-39.9
$\infty$	3.314	4.005	-17.3	8.912	13.65	-34.7	10.03	16.72	-40.0

## 4.0 Two-Dimensional Modeling

Two two-dimensional models have been developed to analyze a substrate with symmetrical heat sources. Steady-state temperatures over the substrate surface are then calculated. A cross-sectional (or slice) model examines the temperature variation through the thickness of the substrate with varying values of resistance to heat flow below the substrate, as shown in Fig. 8. No spreading of heat into the plane of the slice is accounted for, so this model effectively assumes that the heat source is a long strip. A slab model assumes the temperature gradient through the thickness of the substrate is small, as shown in Fig. 9. The two models are compared to a two-dimensional axisymmetric solution for accuracy. The two-dimensional models created may be an effective way to analyze steady-state temperature distributions in hybrid substrates with interaction between symmetrically spaced heat sources.



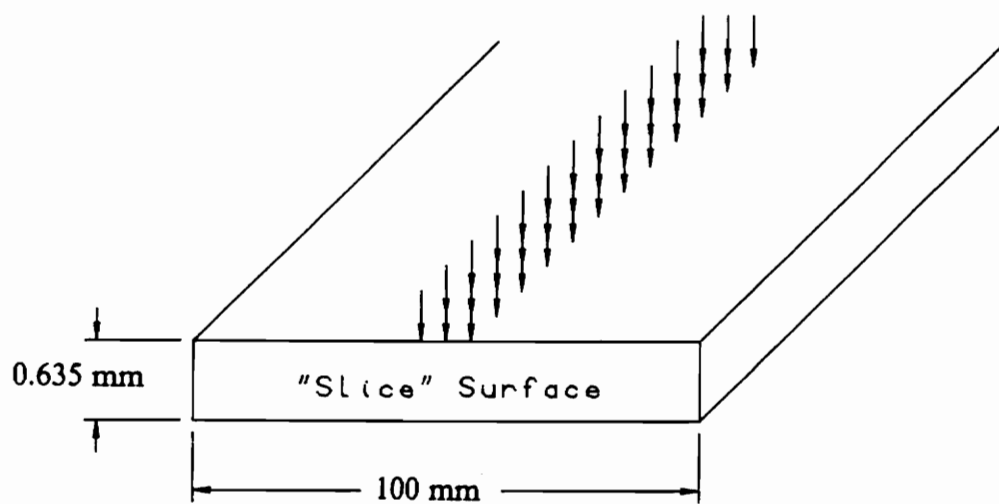
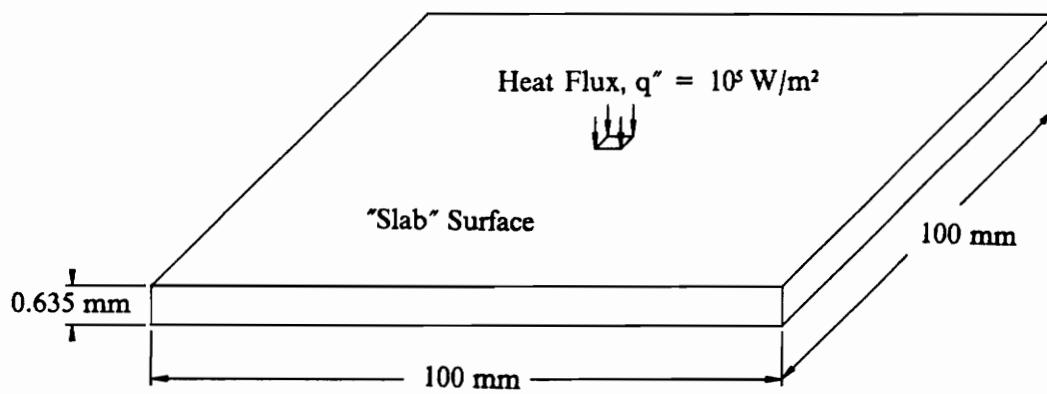


Figure 8. Slice model used in HEAT



**Figure 9.** Slab model used in TASS

## ***4.1 Slice Model***

The program HEAT analyzes the temperature distribution through the thickness of a substrate resulting from a heat flux of infinite length into the plane of the slice. Because the heat source is infinitely deep, heat only spreads down and across the slice and not into or out of the plane of the slice. To check convergence of the model, an energy balance is performed relating the heat input to the heat output. Taking into consideration this energy balance as well as computer run time, a practical convergence criterion and nodal grid have been established. The value of the resistance to heat flow below the substrate, representing a heat sink to ambient air, is varied from 0.007257 to 4.0 K/W.

To solve for the temperature distribution, the governing differential equation for two-dimensional heat conduction is modeled by a control-volume based finite-difference method. The resulting algebraic equations are then implemented in a FORTRAN code. This process has inherent discretization errors due to a finite  $\Delta x$ . The algebraic equations are solved using Gauss-Seidel iteration by converging the solution to a given tolerance. This process has inherent convergence errors which can only approach the roundoff error level. By comparing solutions on successively finer grids, the discretization error can be estimated as shown in Table 2. A grid was chosen to reduce this error to less than approximately 1 K. A tolerance was chosen so the program will converge to less than one percent energy balance error. The solution has an accuracy based on the larger error, so reducing one type of error much smaller than the other is unnecessary.

Table 2. Comparison of grids to estimate discretization error

21 × 5 Grid				61 × 5 Grid				61 × 15 Grid			
Resistance (K/W)	Energy Bal. Error (%)	Max. Temp. (K)	Max. Temp. Gradient (K)	Energy Bal. Error (%)	Max. Temp. (K)	Max. Temp. Gradient (K)	Energy Bal. Error (%)	Max. Temp. (K)	Max. Temp. Gradient (K)	Energy Bal. Error (%)	Max. Temp. Gradient (K)
0.4	0.507	356.89	1.41	0.528	355.88	1.40	1.49	355.80	1.40	1.49	1.40
0.533	0.576	368.37	1.36	0.611	367.18	1.36	1.67	367.09	1.35	1.67	1.35
0.8	0.667	387.76	1.30	0.680	386.31	1.29					
1.6	0.845	431.14	1.20	0.907	429.24	1.20					
4.0	1.13	511.75	1.10								

The formulation of algebraic nodal equations for this model uses a uniform grid in each direction, but the size of each element does not have to be the same in each direction. Test cases were run using  $21 \times 5$ ,  $61 \times 5$ , and  $61 \times 15$  grids. The grids show similar energy balance errors, with the  $61 \times 15$  grid having the highest errors at the same convergence criterion. The grids also showed similar maximum temperatures to within 1 K and similar maximum temperature gradients to within 0.01 K. In addition to this, as the control volumes within a grid are made smaller, the computer time required to converge the solution to a specified tolerance increases. At the same tolerance, the  $61 \times 15$  grid takes much longer to run than the  $21 \times 5$  grid yet produces approximately the same results. Therefore, the  $21 \times 5$  grid is used since it is the most practical.

A tolerance is chosen to obtain low energy balance error consistent with the discretization error and low run time. The value is chosen by plotting graphs comparing percent error with tolerance for several values of resistance, as shown in Fig. 10. The graphs all level off at a tolerance of approximately  $10^{-4}$ . This convergence value is not unnecessarily small when compared to the discretization error yet yields an energy balance error of less than one percent for the various values of resistances tested.

Using a nodal grid of  $21 \times 5$  and a tolerance of  $10^{-4}$ , maximum temperatures and temperature gradients are determined from the program HEAT, as shown in Table 2. The maximum temperature gradient is defined as the difference between the maximum temperature and the temperature at the bottom of the substrate directly below the maximum temperature. These numbers are conservative if the actual heat source is square or rectangular because this two-dimensional model considers the heat source to be infinite into

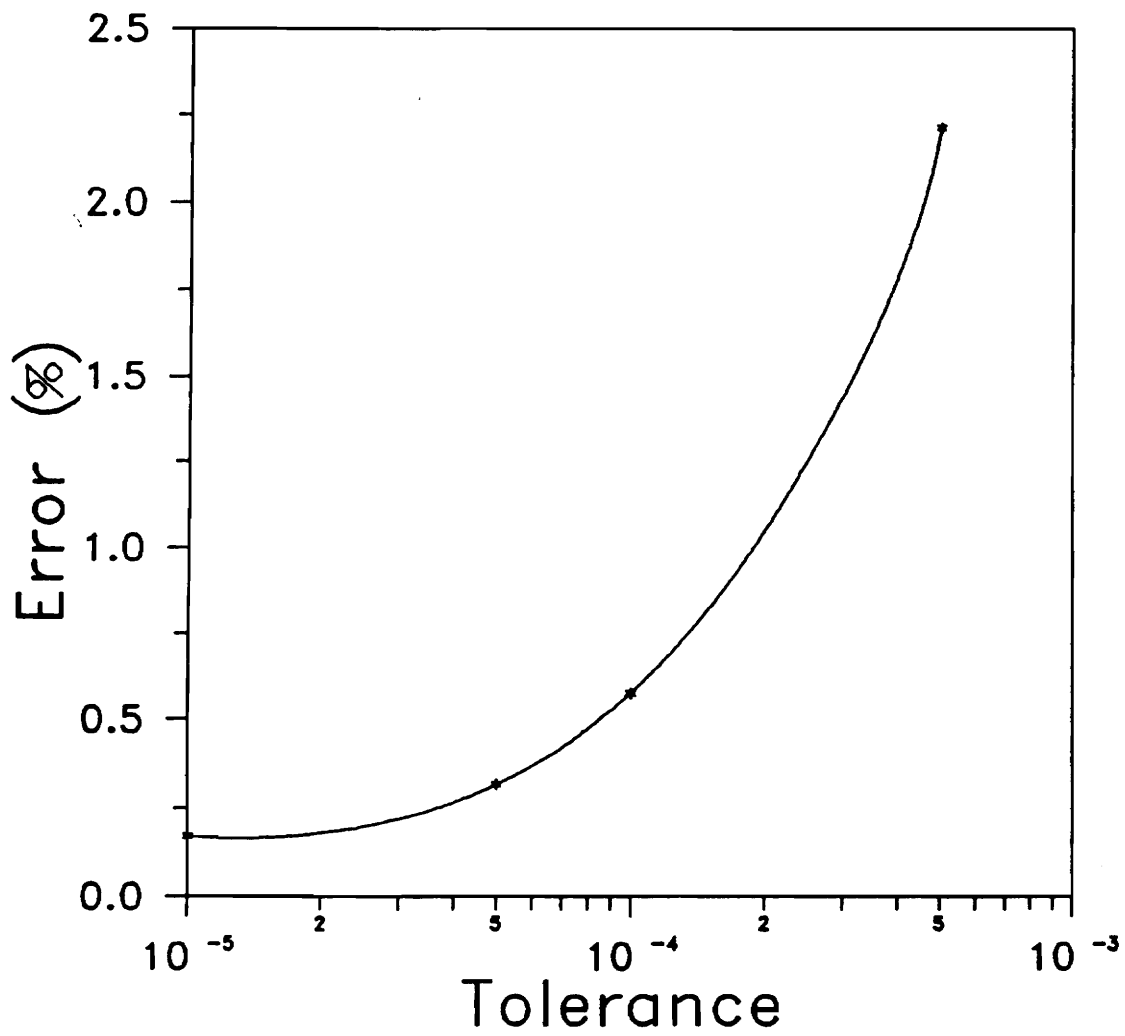


Figure 10. Tolerance values in HEAT

the plane of the slice. The HEAT model also shows that the temperature gradient through the thickness of the substrate is of the order of 1 K for the geometry and heat source strength considered. Thus, the assumption in the slab model that the temperature gradient through the thickness of the substrate is small may be valid.

A Biot number provides a one-dimensional measure of the temperature drop in a solid relative to the temperature difference between the solid surface and the ultimate heat sink temperature. By changing the resistance below the substrate, several Biot numbers were obtained for the program HEAT. Because the heat spreads through the substrate two-dimensionally, the Biot number is only approximately the ratio of temperature drop through the substrate to temperature drop below the substrate,  $\frac{T_{\max} - T_{hs}}{T_{hs} - T_0}$ .

As the ratio of temperatures approaches the Biot number, the heat flow through the substrate approaches one-dimensionality for this particular geometry, as shown in Table 3, because resistance below the substrate decreases relative to the resistance through the substrate. When the resistance is 0.4 K/W, the Biot number is 0.0181, the largest temperature gradient is 1.41 K from a maximum temperature of 356.89 K and the ratio of temperature differences is 0.025. When the resistance is lowered to 0.00726 K/W, holding the substrate thickness and conductivity constant, the Biot number increases to 1.0 and the ratio of temperatures is 1.01. The largest temperature gradient increases to 1.80 K at a maximum temperature of only 303.59 K. Therefore, as the Biot number increases, the heat flow through the substrate becomes more one-dimensional but the temperature gradient through the thickness of the substrate becomes more significant.

Table 3. Comparison of Biot number to temperature difference ratio

Biot Number	External Resistance (K/W)	Max. Temp. (K)	Max. Temp. Change (ΔK)	$\frac{T_{s1} - T_{s2}}{T_{s2} - T_0}$
0.0181	0.4	356.89	1.41	0.0254
0.1	0.0726	317.03	1.67	0.1087
1.0	0.00726	303.59	1.80	1.006



## 4.2 *Slab Model*

The program TASS analyzes the temperature distribution across the substrate, assuming that the temperature gradient through the thickness of the substrate is negligible, as shown in Fig. 9. Two heat fluxes are applied symmetrically to the substrate. Heat then conducts two-dimensionally along the slab, convects to ambient air from the top of the substrate and conducts to a heat sink below the substrate. The governing differential equations are modeled by a control-volume based finite-difference method. The resulting algebraic equations are implemented in a FORTRAN code using line-by-line Gauss-Seidel iteration with over-relaxation and a tridagonal matrix solver. This method is significantly more efficient than point-by-point Gauss-Seidel iteration by itself. As in HEAT, an energy balance is used to check convergence of the iterative solution.

Due to the formulation of algebraic equations for the model, the control volumes in TASS must be square. To match HEAT, two nodal grids were analyzed:  $21 \times 21$  and  $61 \times 61$ . Both grids show energy balance errors of less than one percent. However, the  $61 \times 61$  grid predicts maximum temperatures about 2 K lower than the  $21 \times 21$  grid, as shown in Table 4. The 2 K difference is fairly significant, but the  $21 \times 21$  grid is chosen as best to match results in HEAT.

As with HEAT, several levels of convergence criterion were tested in TASS. For a range of  $10^{-4}$  to  $10^{-7}$ , the energy balance error is approximately the same. Above  $10^{-4}$ , error

Table 4. Comparison of grids in TASS to estimate discretization error

21 × 21 Grid			61 × 61 Grid		
External Resistance (K/W)	Energy Balance Error (%)	Max. Temp. (K)	Energy Balance Error (%)	Max. Temp. (K)	
0.4	0.185	310.29	0.782	308.47	
0.533	0.294	310.97	2.15	309.08	
0.8	0.132	311.91	0.140	309.94	
1.6	0.306	313.45	0.276	311.39	
4.0	0.103	315.34	0.775	313.20	

increases quadratically. Because run time is not significantly different between criteria of  $10^{-4}$  and  $10^{-7}$ , a value of  $10^{-6}$  is chosen as the convergence criterion.

### 4.3 Results

Results from HEAT are compared to axisymmetric results, as with the one-dimensional model discussed previously. The two models are compared over a wide range of substrate thicknesses and Biot numbers. The substrate area is held constant at a B of four. Results of HEAT are accurate when A is 0.1 and the Biot number is large, as shown in Table 5. Otherwise, like the one-dimensional results, HEAT results are generally inaccurate but are accurate under certain conditions. For example, at  $A = 0.5$ ,  $B = 4.0$  and  $Bi = 0.01$ , the error is only +4.76%. If the Biot number is changed to 1.0, the error jumps to +25.0%. Like the one-dimensional results, total resistances are compared to eliminate the dependency of the magnitude of the result on the heat source power.

TASS is also compared to axisymmetric results for accuracy. Again, the models are compared over a wide range of thicknesses and Biot numbers. Two values of B are considered: four and twenty. Like other models compared to axisymmetric results, the results from TASS are not very accurate, as shown in Table 6 for  $B = 4$  results and Table 7 for  $B = 20$  results. Because of the nature of the model, it is expected to be accurate when the substrate is thin and the Biot number is small. When  $A = 0.1$ ,  $Bi =$

Table 5. Accuracy of IIEAT results vs. axisymmetric model results

Bi	A = 0.1				A = 0.5				A = 1.0			
	$R_{tot,HT}$ (K/W)		$R_{tot,A,XI}$ (K/W)		$R_{tot,HT}$ (K/W)		$R_{tot,A,XI}$ (K/W)		$R_{tot,HT}$ (K/W)		$R_{tot,A,XI}$ (K/W)	
0.01	29.45	8.053	+266		16.16	15.42			14.10	28.73		-50.9
1.0	1.569	0.8319	+88.6		2.291	1.833			2.859	2.106		+35.8
100.0	0.4411	0.4337	+1.71		1.740	1.464			2.548	1.797		+41.8
$\infty$	0.4286	0.4293	-0.163		1.734	1.458			2.545	1.793		+41.9

Table 6. Accuracy of TASS results vs. axisymmetric model results, B=4

A = 0.1				A = 0.5				A = 1.0			
Bi	R <sub>tot,TASS</sub> (K/W)	R <sub>tot,AXI</sub> (K/W)	% Error	R <sub>tot,TASS</sub> (K/W)	R <sub>tot,AXI</sub> (K/W)	% Error	R <sub>tot,TASS</sub> (K/W)	R <sub>tot,AXI</sub> (K/W)	% Error		
0.01	22.32	24.16	-7.62	16.05	46.27	-65.3	23.23	86.18	-73.0		
1.0	0.78	2.495	-69	2.58	5.499	-53.1	2.24	6.319	-64.6		
100.0	0.016	1.301	-99	0.064	4.391	-99	0.13	5.391	-98		

Table 7. Accuracy of TASS results vs. axisymmetric model results, B=20

Bi	A = 0.1			A = 0.5			A = 1.0		
	$R_{tot,TASS}$ (K/W)	$R_{tot,AXI}$ (K/W)	% Error	$R_{tot,TASS}$ (K/W)	$R_{tot,AXI}$ (K/W)	% Error	$R_{tot,TASS}$ (K/W)	$R_{tot,AXI}$ (K/W)	% Error
0.01	27.94	22.68	+ 23.2	22.91	11.75	+ 95.0	6.86	10.76	-36.2
1.0	1.23	2.495	-50.7	8.82	5.481	+ 60.9	2.80	5.970	-53.1
100.0	0.016	1.301	-99	1.25	4.391	-71.5	0.13	5.363	-98

0.01 and  $B = 4.0$ , the error is only -7.61%. However, when  $B$  changes to twenty, the error increases to +23.19%. The difference in signs of the two errors indicated that some  $B$  exists where the two models match exactly. Like the one-dimensional results, accurate solutions would be needed to determine what that  $B$  is.

The two two-dimensional models described above require some sort of computer code to be practical. The code can be as simple as a finite difference routine or as complex as a finite element code. The program can be run on a personal computer and can calculate a temperature distribution relatively quickly. Unfortunately, results are generally inaccurate. The heat flux path varies under different boundary conditions, creating the need for a radial or three-dimensional model. An axisymmetric model, described in the following chapter, allows for radial heat spreading while keeping the analysis two-dimensional. Therefore, the axisymmetric model is recommended in place of the slice and slab models presented above.

## 5.0 Axisymmetric Modeling

An axisymmetric model has been developed to investigate the effects of heat source interaction on a substrate. The results predict the maximum temperature of the device for a spectrum of geometries and boundary conditions. This model can be applied to practical designs of hybrid power supplies to analyze thermal interaction.

The model divides the problem into a series of two resistances: the resistance of the substrate and the resistance of everything external to the substrate. This external resistance includes the resistance of the bond to the heat sink, the heat sink and the convection from the heat sink to air. The model is reduced to three nondimensional parameters. The thickness and width of the substrate may be independently varied from very thin and narrow to semi-infinite. Also, the Biot number, which incorporates the external resistance below the substrate, allows for a wide variety of boundary conditions below the substrate. The spreading resistance through the substrate is calculated from



a two-dimensional axisymmetric finite element solution for the temperature distribution in the substrate. The results are valid for a general substrate conductivity, allowing comparison between different substrate materials such as alumina and aluminum nitride.

## **5.1 *Dimensional Model***

A circuit operates with a variety of transient current waveforms. These oscillations of current are so fast that the system can be thermally modeled as steady-state. A silicon die has high thermal conductivity relative to the substrate, which allows heat generated at the junctions to spread through the device before entering the substrate. In the axisymmetric model, the heat generated within the device is modeled as a steady-state, uniform flux on the top surface of the substrate, with an area equal to that of the device. The temperature rise through the device and die attach layer, including any voiding or contact resistance, can be approximated and added to the results given here, though this portion of the temperature rise is often small compared to the total temperature rise.

The bottom side of the substrate is bonded to some form of a solid heat sink. The total thermal resistance, including fin effectiveness and convection, of standard air-cooled heat sinks can be found from manufacturer's data for natural convection and for forced convection as a function of air flow rate and air density or altitude. Other types of heat sinks will require some analysis to estimate the total thermal resistance. The bond material between the substrate and heat sink usually has much lower thermal conductivity

than the heat sink (even for a "thermally conductive" epoxy). The bond layer will thus cause the thermal resistance below the substrate to be relatively evenly distributed over the area of the substrate. For the model, the total external resistance below the substrate is replaced by an equivalent heat transfer coefficient at the bottom surface of the substrate. Note that the equivalent heat transfer coefficient should relate the total external resistance to the area of the substrate occupied by one device:

$$h_{eq} = \frac{1}{R_{ext}A_{sub}} \quad [5.1]$$

The majority of heat generated in a hybrid circuit is conducted through the substrate and into the heat sink. Convection and radiation heat transfer directly from the top surface of the substrate will normally account for less than 5% of the total dissipation. A lid or cover over the circuit will further reduce these modes of heat transfer. The top surface is thus modeled as insulated except where a device produces a heat flux.

The devices on the substrate are modeled as being symmetrically spaced, as shown in Fig. 11. These lines of symmetry combine with the (assumed) insulated edges of the substrate to produce a region with adiabatic or insulated sides. The width of the insulated region is determined by the spacing between devices. To properly solve the problem for this geometry requires a three-dimensional analysis. However, Negus et al. (1989) and Kadambi and Abuaf (1983) have shown that an equivalent two-dimensional axisymmetric model provides very accurate results. Rectangular devices with aspect ratios of up to three placed eccentrically from the center of the insulated region by a factor of up to one-half changed the thermal resistance in Kadambi's and Abuaf's (1983) re-

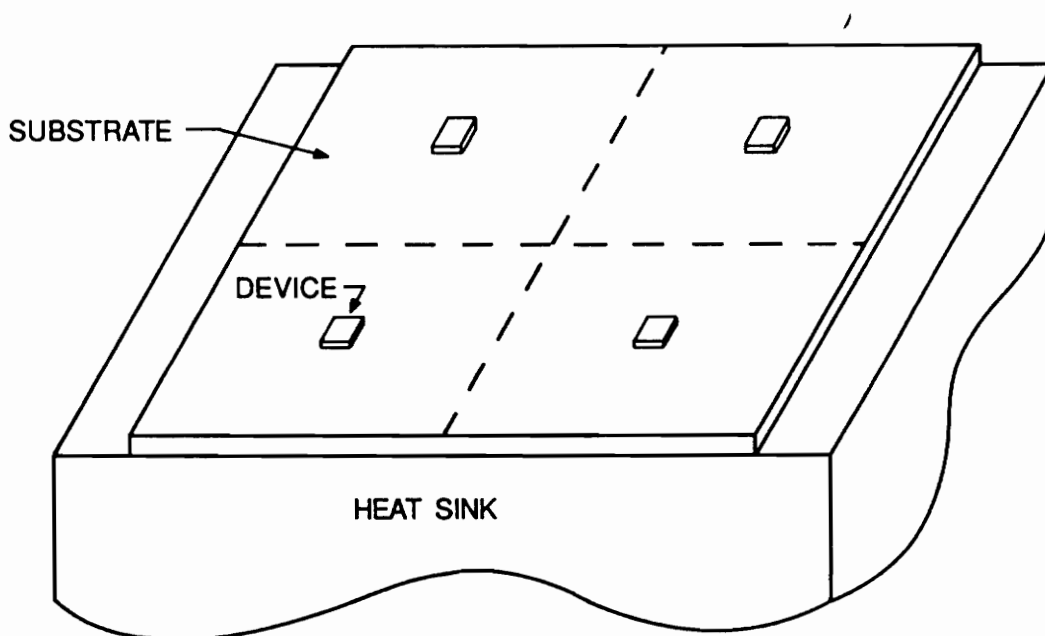


**Figure 11. Symmetrically spaced heat sources on a substrate and heat sink**

sults by about 5% relative to the axisymmetric case. An axisymmetric approximation, shown in Fig. 12, is used in this work. Note that a two-dimensional axisymmetric approximation is more appropriate than a two-dimensional planar approximation for this three-dimensional problem. The two-dimensional planar approximation is strictly valid only for a long strip heat source with no spreading in the third cartesian dimension.

Many practical problems do not have a symmetric pattern of devices. The results presented here provide a conservative estimate of thermal interaction in terms of a minimum number of parameters and allow the development of design rules suitable for preliminary layout of hybrid circuits.

The physical problem defined above is modeled as a circular, uniform heat flux acting on a cylindrical section of substrate which is insulated on all sides except the bottom. The bottom of the substrate is cooled by convection. The governing equation for this steady-state model is

$$\frac{1}{r} \frac{d}{dr} \left( r \frac{dT}{dr} \right) + \frac{d^2T}{dz^2} = 0 \quad [5.2]$$

with boundary conditions

$$\frac{dT}{dr} (0,z) = 0 \quad [5.3]$$

$$\frac{dT}{dr} (r_b,z) = 0 \quad [5.4]$$

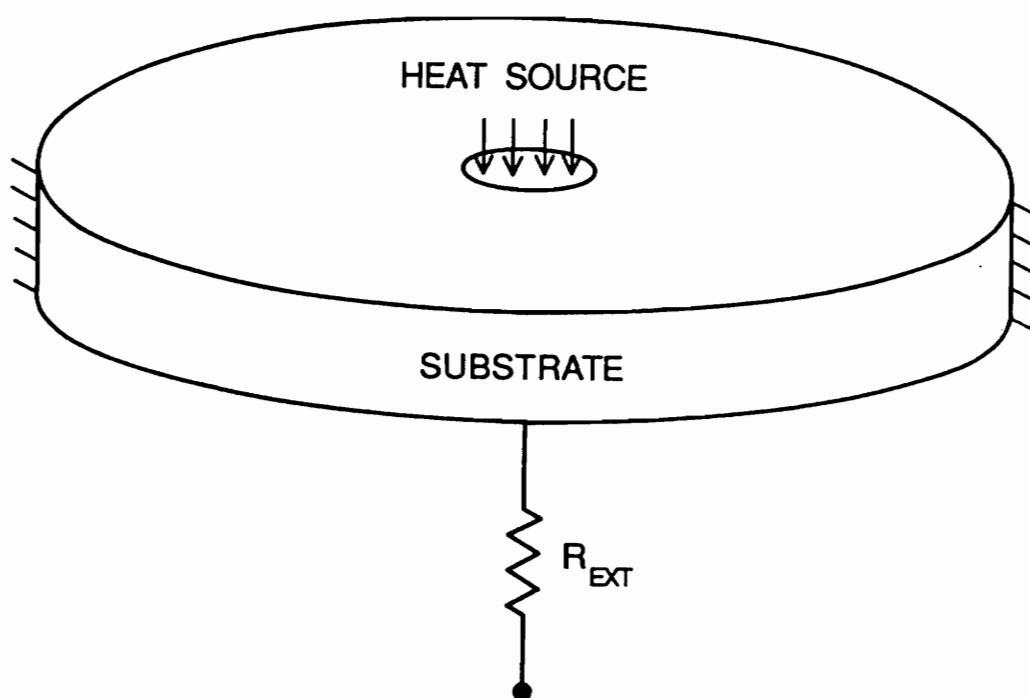


**Figure 12.** Axisymmetric approximation of one source on a substrate

$$\frac{dT}{dz}(r_d < r < r_b, 0) = 0 \quad [5.5]$$

$$-k \frac{dT}{dz}(0 < r < r_d, 0) = q_d'' \quad [5.6]$$

$$-k \frac{dT}{dz}(r, t) = h_{eq}[T(r, t) - T_0] \quad [5.7]$$

These conditions are illustrated in Figure 13.

## 5.2 Nondimensionalization

The dimensional form of the governing equations contains seven independent parameters: thermal conductivity, heat source strength, source radius, substrate radius, substrate thickness, external resistance, and ambient temperature. To reduce the model to three independent parameters, the governing equation and boundary conditions are converted to nondimensional variables. The equivalent diameter of the heat source is selected as a length scale. The variable  $A$  represents the thickness of the substrate in terms of the diameter,  $d$ .  $B$  represents the width in terms of  $d$ . This distance is determined by spacing between devices or spacing to the edge of the substrate.  $Bi$  is the Biot number, which represents the relative thermal coupling to the heat sink medium. The nondimensional governing equation reduces to

$$\frac{1}{R} \frac{d}{dR} \left( R \frac{d\theta}{dR} \right) + \frac{d^2\theta}{dZ^2} = 0 \quad [5.8]$$

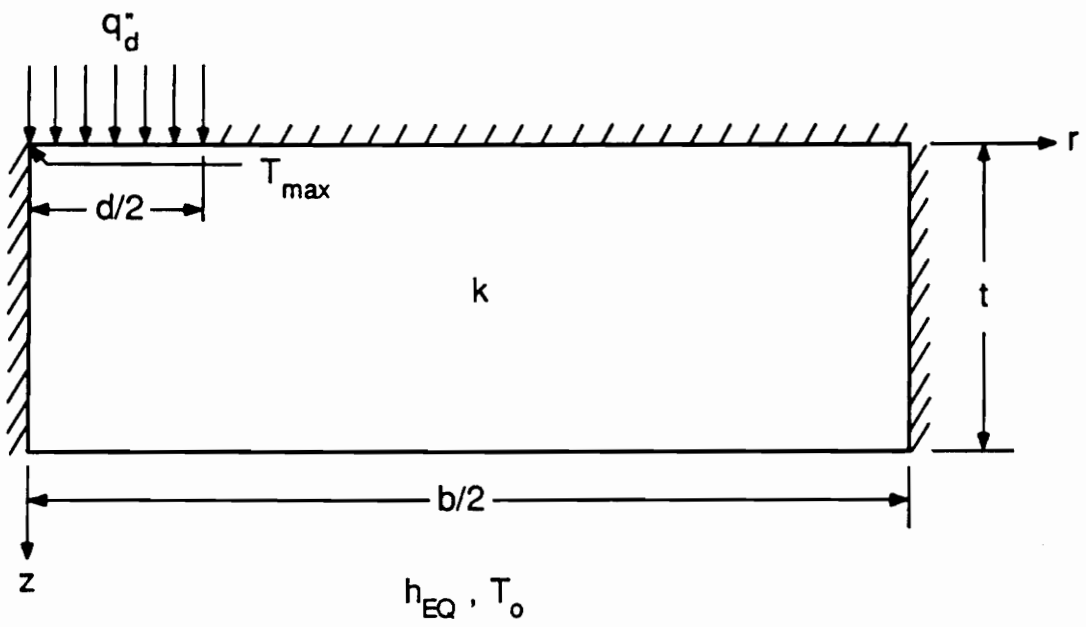


**Figure 13. Dimensional axisymmetric model**

with nondimensional boundary conditions

$$\frac{d\theta}{dR}(0,Z) = 0 \quad [5.9]$$

$$\frac{d\theta}{dR}\left(\frac{B}{2},Z\right) = 0 \quad [5.10]$$

$$\frac{d\theta}{dZ}\left(\frac{1}{2} < R < \frac{B}{2},0\right) = 0 \quad [5.11]$$

$$\frac{d\theta}{dZ}\left(0 < R < \frac{1}{2},0\right) = -1 \quad [5.12]$$

$$\frac{d\theta}{dZ}(R,A) = \frac{-Bi}{A} \theta(R,A) \quad [5.13]$$

The nondimensional model is illustrated in Figure 14. This model could be solved analytically in terms of infinite series or numerically by discretizing the problem. The finite element method was chosen because it is an accurate method which may be solved using one of several commercially available computer software packages. To insure accuracy, the finite element mesh was refined for each geometry until the results showed no change to four significant digits.

The two-dimensional, axisymmetric model can be thought of as a resistance network. Symmetry conditions create "flux tubes" around the device. A constant heat flux enters the top and creates a maximum temperature at the center of the device. The flux spreads through the substrate, encountering a resistance. The average temperature at the interface of the substrate and the heat sink varies depending on the resistance of the heat



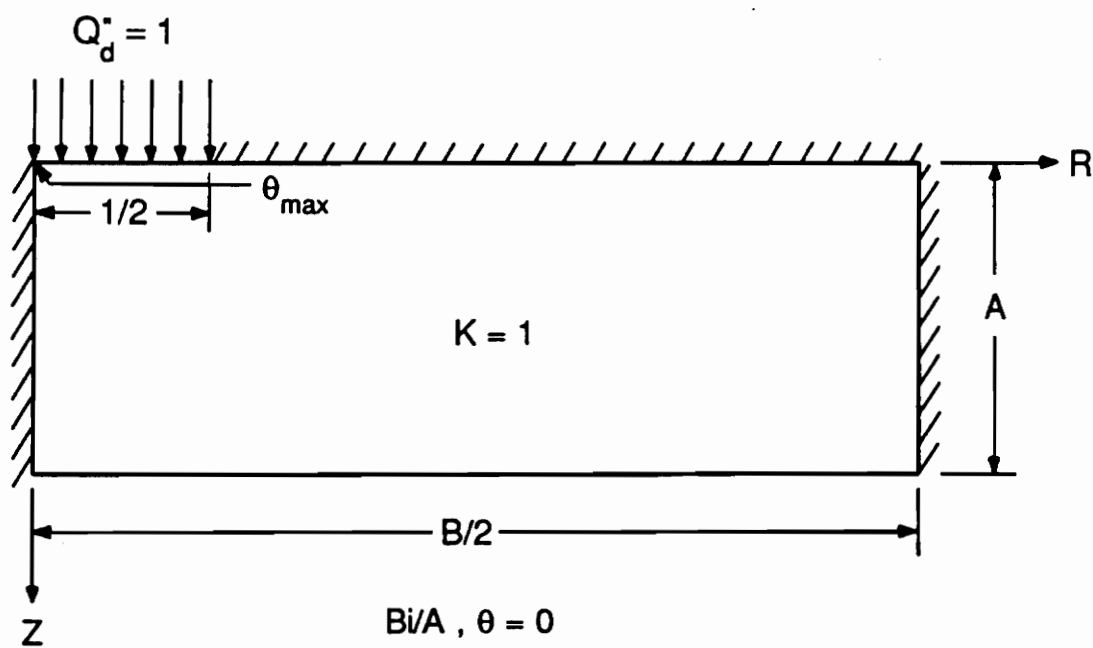


Figure 14. Nondimensional axisymmetric model

sink. The temperature of the fluid cooling the heat sink represents the atmospheric or environment temperature, and is zero since it is used as reference temperature. Thus, the model is broken down into two lumped resistances in series: the spreading resistance of the substrate and the resistance of everything external to the substrate.

The equivalent thermal resistance network is shown in Figure 15. Starting from the basic definition of thermal resistance,

$$q_d'' A_d = \frac{T_{\max} - T_0}{R_{\text{tot}}} = \frac{T_{\max} - T_0}{R_{\text{sp}} + R_{\text{ext}}} \quad [5.14]$$

and converting to a nondimensional form in terms of  $\theta_{\max}$  yields:

$$\Phi_{\text{sp}} = k\sqrt{A_d} R_{\text{sp}} = \frac{1}{\sqrt{\pi/4}} \theta_{\max} - \frac{1}{\sqrt{\pi/4}} \frac{A}{B^2 \text{Bi}} \quad [5.15]$$

$$\Phi_{\text{ext}} = k\sqrt{A_d} R_{\text{ext}} = \frac{1}{\sqrt{\pi/4}} \frac{A}{B^2 \text{Bi}} \quad [5.16]$$

$$\Phi_{\text{tot}} = k\sqrt{A_d} R_{\text{tot}} = \frac{1}{\sqrt{\pi/4}} \theta_{\max} \quad [5.17]$$

The square-root of the device area has been used to express the nondimensional spreading resistance,  $k\sqrt{A_d} R_{\text{sp}}$ . This form was suggested by Negus et al. (1989) for the constriction resistance used in semi-infinite regions. Expressing the spreading resistance in this form allows the results presented in the next section to be applied for any device

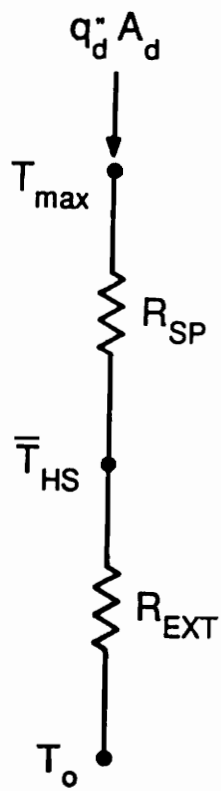


Figure 15. Equivalent thermal network of the axisymmetric model

heat flux,  $q_d''$ , a variety of device shapes and sizes, and any substrate thermal conductivity.

## 6.0 Results of Axisymmetric Modeling

Results of the axisymmetric model, solved using a finite element analysis, yield the maximum temperature at the center of the heat source. The three parameters, width,  $B$ , thickness,  $A$ , and Biot number,  $Bi$ , are defined for each case. With these parameters specified, the resistance through the substrate, the resistance below the substrate, and the average temperature between the substrate and the heat sink can be calculated. A comprehensive list of maximum temperatures for a wide range of the three parameters is presented in Table 8. A list of spreading resistances through the substrate for the same variation of the parameters is presented in Table 9. A design example explains how to use these values. This chapter describes the effect each parameter has on maximum temperature and illustrates some trends in the results.

Table 8. Nondimensional maximum temperatures

B1	B = 1.0	1.6	2.4	4	8	12	20
	A = 0.1						
.01	10.1	4.346	2.550	1.873	1.760	1.759	1.759
.1	1.1	0.7263	0.6783	0.6745	0.6745	0.6745	0.6745
1	0.2	0.1935	0.1935	0.1935	0.1935	0.1935	0.1935
10	0.11	0.1097	0.1097	0.1097	0.1097	0.1097	0.1097
100	0.101	0.1009	0.1009	0.1009	0.1009	0.1009	0.1009
-	0.1	0.09988	0.09988	0.09988	0.09988	0.09988	0.09988
	A = 0.5						
.01	50.5	19.90	9.061	3.588	1.391	1.043	0.9113
.1	5.5	2.318	1.246	0.7628	0.6294	0.6221	0.6215
1	1.0	0.5587	0.4514	0.4264	0.4250	0.4250	0.4250
10	0.55	0.3792	0.3545	0.3521	0.3521	0.3521	0.3521
100	0.505	0.3604	0.3420	0.3405	0.3405	0.3405	0.3405
-	0.5	0.3583	0.3405	0.3391	0.3391	0.3391	0.3391
	A = 1.0						
.01	101.0	39.62	17.81	6.683	2.049	1.224	0.8347
.1	11.0	4.464	2.184	1.057	0.6353	0.5807	0.5664
1	2.0	0.9478	0.6207	0.4900	0.4636	0.4629	0.4629
10	1.1	0.5963	0.4636	0.4259	0.4225	0.4225	0.4225
100	1.01	0.5611	0.4476	0.4180	0.4159	0.4159	0.4159
-	1.0	0.5572	0.4459	0.4171	0.4150	0.4150	0.4150
	A = 2.0						
.01	202.0	79.07	35.34	12.99	3.592	1.869	1.005
.1	22.0	8.760	4.093	1.738	0.7787	0.6173	0.5493
1	4.0	1.729	0.9675	0.6125	0.4948	0.4835	0.4816
10	2.2	1.026	0.6550	0.4998	0.4624	0.4609	0.4608
100	2.02	0.9556	0.6237	0.4884	0.4583	0.4573	0.4573
-	2.0	0.9478	0.6203	0.4872	0.4579	0.4569	0.4569
	A = 5.0						
.01	505.0		87.95	31.92	8.322		
1	10.0		2.009	0.9874	0.5872		
-	5.0		1.141	0.6749	0.5090		
	A = 10.0						
.01	1010.	394.9	175.9	63.49	16.21	7.468	2.998
.1	110.0	43.30	19.64	7.238	2.150	1.218	0.7476
1	20.0	8.146	4.018	1.613	0.7437	0.5930	0.5226
10	11.0	4.630	2.456	1.050	0.6030	0.5305	0.5001
100	10.1	4.278	2.300	0.9939	0.5890	0.5243	0.4979
-	10.0	4.239	2.282	0.9877	0.5874	0.5236	0.4976

Table 9. Nondimensional spreading resistances

Bi	B = 1.0	1.6	2.4	4	8	12	20
	A = 0.1						
.01	0.1128	0.4958	0.9178	1.409	1.810	1.906	1.956
.1		0.3788	0.5695	0.6906	0.7435	0.7533	0.7583
1		0.1743	0.1988	0.2113	0.2166	0.2176	0.2181
10		0.1194	0.1218	0.1231	0.1236	0.1237	0.1238
100		0.1134	0.1137	0.1138	0.1138	0.1138	0.1139
∞	v	0.1127	0.1127	0.1127	0.1127	0.1127	0.1127
	A = 0.5						
.01	0.5642	0.4124	0.4294	0.5223	0.6884	0.7846	0.8872
.1		0.4122	0.4268	0.5081	0.6220	0.6628	0.6872
1		0.4100	0.4114	0.4459	0.4707	0.4756	0.4782
10		0.4058	0.3902	0.3938	0.3964	0.3969	0.3972
100		0.4045	0.3849	0.3839	0.3841	0.3842	0.3842
∞	v	0.4043	0.3842	0.3826	0.3826	0.3826	0.3826
	A = 1.0						
.01	1.128	0.6288	0.5049	0.4886	0.5485	0.5971	0.6600
.1		0.6288	0.5049	0.4877	0.5406	0.5769	0.6109
1		0.6288	0.5045	0.4824	0.5055	0.5145	0.5195
10		0.6288	0.5035	0.4735	0.4750	0.4760	0.4765
100		0.6287	0.5031	0.4710	0.4691	0.4692	0.4693
∞	v	0.6287	0.5031	0.4707	0.4683	0.4683	0.4683
	A = 2.0						
.01	2.257	1.070	0.6999	0.5502	0.5265	0.5417	0.5703
.1		1.070	0.6999	0.5502	0.5261	0.5398	0.5634
1		1.070	0.6999	0.5501	0.5231	0.5299	0.5378
10		1.070	0.6999	0.5499	0.5182	0.5185	0.5194
100		1.070	0.6999	0.5497	0.5168	0.5159	0.5160
∞	v	1.070	0.6999	0.5497	0.5167	0.5156	0.5156
	A = 5.0						
.01	5.642		1.288	0.7617	0.5745		
1			1.288	0.7616	0.5744		
∞	v		1.288	0.7616	0.5744		
	A = 10.0						
.01	11.28	4.784	2.575	1.115	0.6629	0.5908	0.5615
.1		4.784	2.575	1.115	0.6629	0.5908	0.5615
1		4.784	2.575	1.115	0.6629	0.5908	0.5615
10		4.784	2.575	1.115	0.6629	0.5908	0.5615
100		4.784	2.575	1.115	0.6629	0.5908	0.5615
∞	v	4.784	2.575	1.115	0.6628	0.5908	0.5614

## ***6.1 Effects of the Biot Number***

The Biot number represents the ratio of resistance to conduction through the substrate and resistance to heat transfer below the substrate. A large Biot number means that resistance below the substrate is much less than resistance through the substrate. Therefore, the heat flux vectors flow mostly downward out of the substrate, where there is less resistance to heat flow, as shown in Fig. 16. A small Biot number means that resistance below the substrate is greater than resistance through the substrate. Heat flux vectors spread radially through the substrate where resistance to heat flow is least before flowing downward and out of the substrate, as shown in Fig. 17.

The spreading of the heat flux in the substrate can be thought of as the heat flow following the path of least resistance. The heat flow spreading in the radial direction increases the active area for dissipation into the heat sink, thus decreasing the resistance by the square of  $B$ . The amount of radial spreading depends on the Biot number, or the relative resistance of the heat sink, and may be limited by the insulated plane of symmetry due to interaction with other devices.

Table 8 shows that as the Biot number increases, the maximum temperature always decreases. A large Biot number also allows closer spacing between heat sources without interaction because the heat flux vectors flow downward. The Biot number, then, clearly effects the two-dimensional distribution of temperature and heat flux within the substrate.



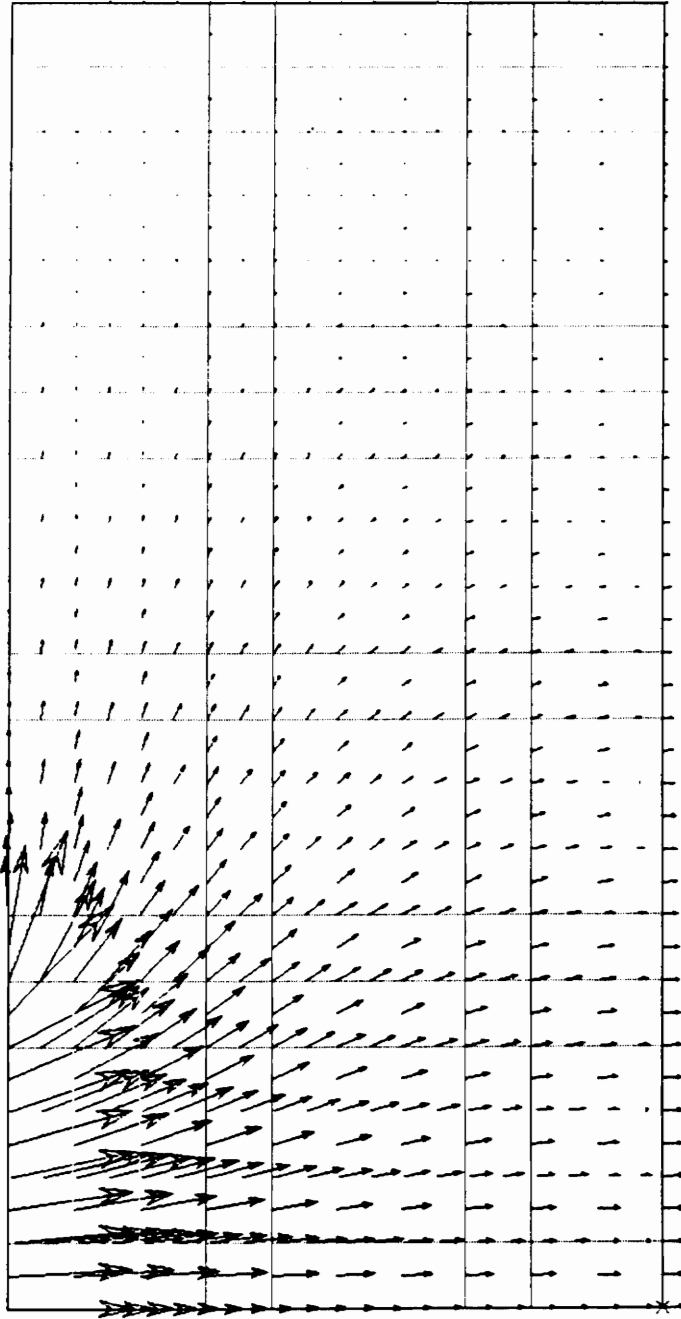


Figure 16. Heat flux through a substrate for a large Biot number

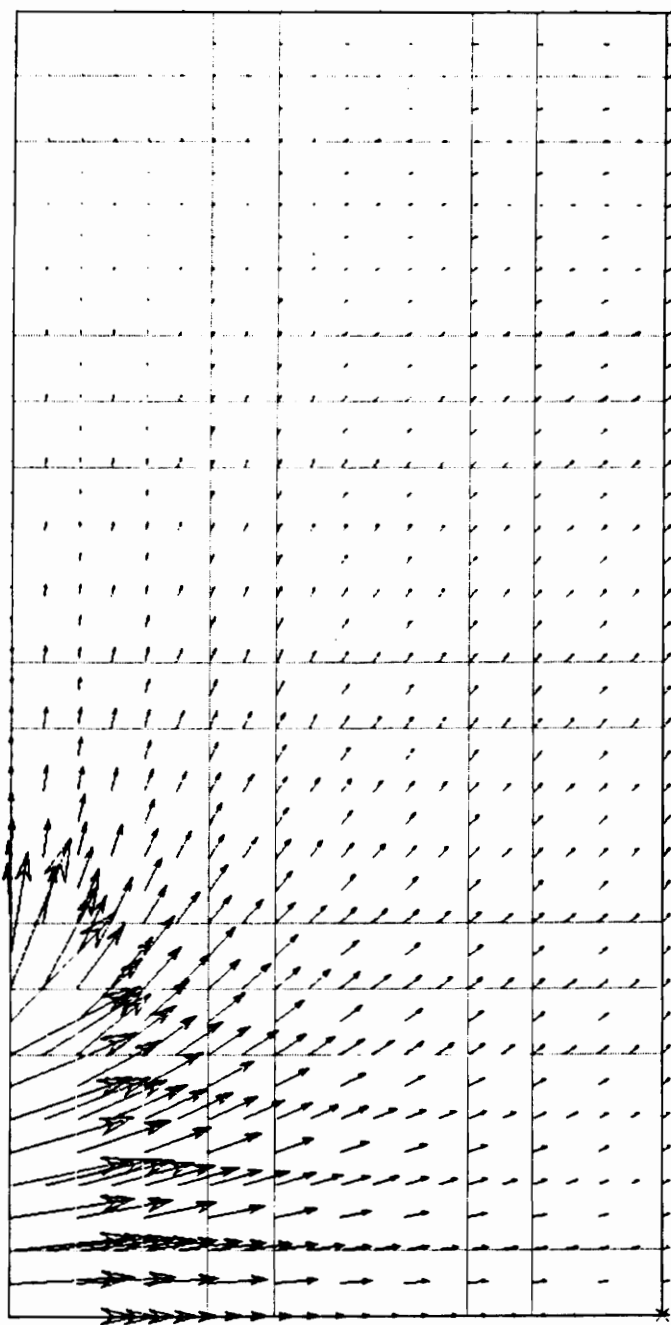


Figure 17. Heat flux through a substrate for a small Biot number

## 6.2 *Effects of the Nondimensional Thickness*

As the parameter  $A$  decreases, both the nondimensional temperature,  $\theta$ , and the nondimensional spreading resistance,  $\Phi$ , decrease for any value of  $B$  and large Biot numbers. When  $B$  is about eight or larger and the Biot number is about 0.1 or smaller, as  $A$  decreases both  $\theta$  and  $\Phi$  initially decrease. This means that, as expected, when the thickness of the substrate is reduced, the resistance to heat transfer through it becomes smaller and the maximum temperature also becomes smaller. Figures 18 and 19 show, however, that when  $A$  is decreased to 0.1,  $\theta$  and  $\Phi$  increase slightly.

Nondimensional temperatures and resistances increase with decreasing  $A$  under certain conditions due to a constriction radially through the substrate. As described above, the heat flux will follow the path of least resistance. A small Biot number causes heat flux to spread radially through the substrate before flowing into the heat sink. A very thin substrate restricts the heat flux from spreading through the substrate because the area for heat transfer is so small, increasing  $\Phi$  and  $\theta$ . Therefore, under some circumstances an optimal  $A$  exists to minimize the maximum temperature. For example, Table 8 shows that for a Biot number of 0.1 and a device spacing of  $B = 8$ , an optimal thickness exists at around  $A = 0.5$ , where  $\theta$  is 0.6294. When  $A$  is 0.1 and 1.0,  $\theta$  is 0.6745 and 0.6353, respectively.

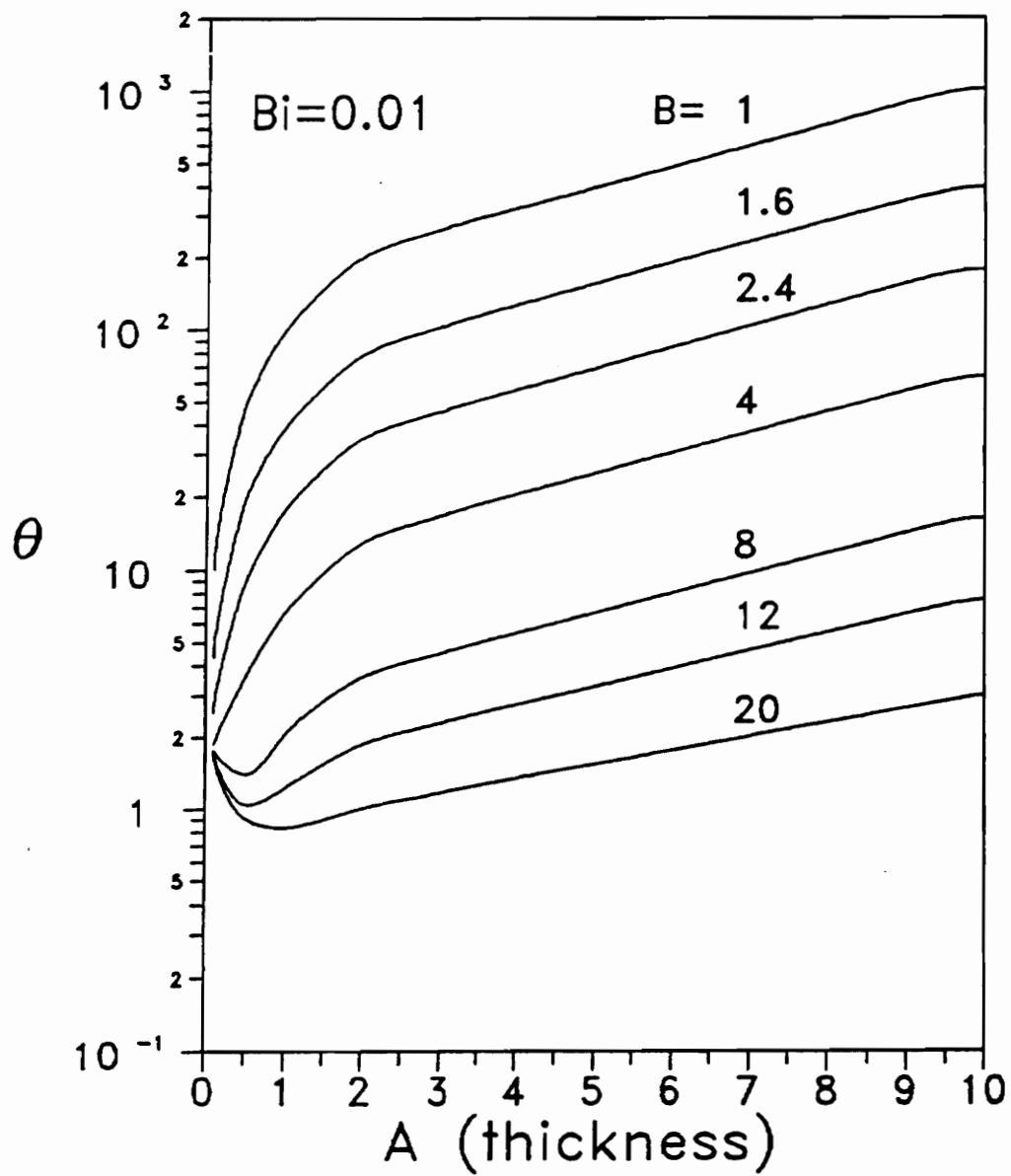


Figure 18. Nondimensional temperature increase at small thicknesses

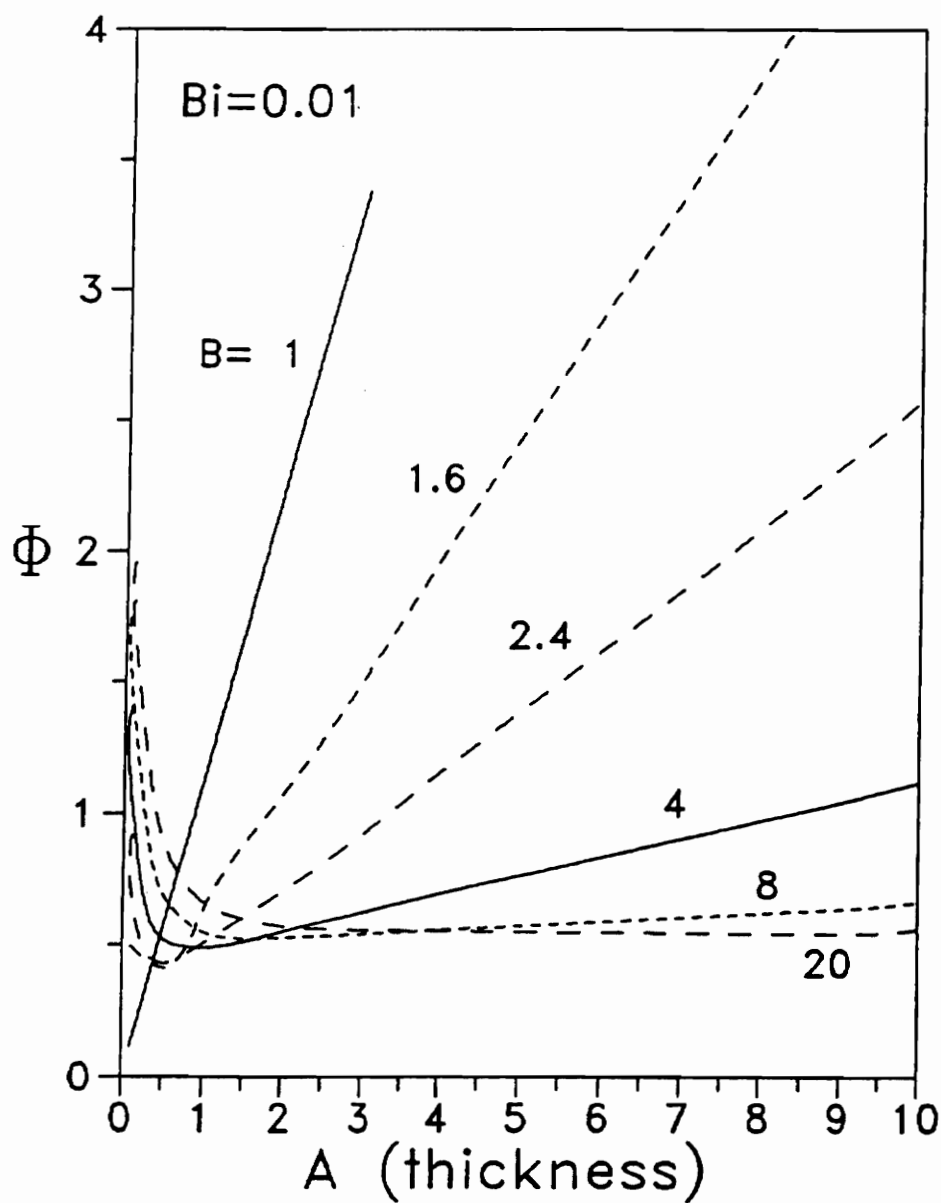


Figure 19. Nondimensional spreading resistance increase at small thicknesses

### ***6.3 Effects of the Nondimensional Width***

As the width parameter,  $B$ , increases  $\theta$  decreases for any thickness,  $A$ , or Biot number. When  $\theta$  does not change with increasing  $B$ , there is no thermal interaction between heat sources. It is of interest to note when  $B$  is large enough to eliminate interaction between adjacent heat sources. Large Biot numbers allow closer heat source spacing without any interaction. For example, when  $A$  is 0.1 and the Biot number is infinity, no interaction occurs when  $B$  is greater than or equal to only 1.6. Smaller, and more practical, Biot numbers require more spacing between sources to eliminate interaction. At the same  $A$  of 0.1 and a Biot number of 0.01, no interaction occurs when  $B$  is greater than eight. Also, smaller thicknesses allow closer heat source spacing without any interaction. When  $A$  is 2.0 and the Biot number is infinity, no interaction occurs when  $B$  is greater than eight. For the same Biot number and an  $A$  of 0.1, no interaction occurs when  $B$  is greater than 1.6.

### ***6.4 Trends in the Results***

Examination of Tables 8 and 9 reveals certain trends in the results. For example, over the range of Biot numbers tested, at a constant  $B$   $\theta$  is linear with the parameter  $A$  when  $A$  is greater than two. Another trend indicates when the geometry is semi-infinite in the width direction. The spreading resistance through the substrate becomes independent of the width parameter,  $B$ , when the thickness parameter  $A$  is about half of  $B$  or greater

and the Biot number is greater than one. Under these conditions, there is no interaction between heat sources. A true semi-infinite condition exists when the width parameter,  $B$ , is greater than twenty and the thickness parameter,  $A$ , is greater than ten.

When  $A$ ,  $B$ , and  $Bi$  are all small, the results show a complex interaction between the heat flow paths in the substrate and the external resistance. A single correlating equation to express these results could not be found. Unfortunately, this is the region of most interest for high-density power hybrid microelectronics.

Nondimensionalization of the model reduces the number of independent parameters from seven to three. Results show that each parameter independently affects temperature rise and resistance through the substrate. Nondimensional temperatures and resistances are tabulated at discrete points over a wide range of practical values. A design example presented in the next chapter explains how to use the results to calculate the maximum temperature created by a source. For more accurate results, a three-dimensional model is necessary.

## 7.0 Design Example

This chapter describes a typical design problem and utilizes the nondimensional results of this work to predict the maximum temperature created by a device on a substrate. Many papers found in the literature review assume an isothermal boundary at the bottom of the substrate. This simplifies the model a great deal, but can lead to inaccurate results. Therefore, the error in assuming an isothermal boundary at the bottom of the substrate is shown. More detailed calculations of the design example and the error of an isothermal boundary assumption are presented in Appendix A.



## 7.1 Maximum Temperature Calculation

Consider a standard alumina ceramic substrate 0.635 mm (0.025 in.) thick with a thermal conductivity of 25 W/m-K. Several devices with equivalent diameters of 6.35 mm (0.25 in.) are placed on the substrate. Each device produces a heat flux of  $4 \times 10^5$  W/m<sup>2</sup>, or a total heat dissipation of 12.7 W. An air-cooled, finned heat sink bonded to the substrate produces an equivalent heat transfer coefficient of 4000 W/m<sup>2</sup>-K when referred back to the area of the substrate. The ambient cooling air is at a temperature of 30°C. We want to calculate the maximum temperature as a function of the device spacing,  $b$ .

To use the present results, we first need to calculate the nondimensional parameters as follows.

$$A = \frac{t}{d} = \frac{0.635 \text{ mm}}{6.35 \text{ mm}} = 0.1 \quad [7.1]$$

$$Bi = \frac{ht}{k} = \frac{(4000 \text{ W/m}^2\text{-K})(0.000635 \text{ m})}{25 \text{ W/m-K}} = 0.1 \quad [7.2]$$

$$B = \frac{b}{d} = 1.0 \text{ to } 20 \quad [7.3]$$

From Table 8, when there is no spacing between sources ( $B = 1$ ), the nondimensional maximum temperature,  $\theta_{\max}$ , is 1.10. The corresponding dimensional temperature is, from the definition of  $\theta$ ,

$$T_{\max} = \theta_{\max} \frac{q_d'' d}{k} + T_0 \quad [7.4]$$

$$T_{\max} = \frac{(1.10)(4 \times 10^5 \text{ W/m}^2)(0.00635 \text{ m})}{25 \text{ W/m-K}} + 30^\circ\text{C} \quad [7.5]$$

$$T_{\max} = 142^\circ\text{C} \quad [7.6]$$

As  $B$  is increased to four, the maximum temperature falls to  $99^\circ\text{C}$ . Increasing  $B$  beyond four does not cause any further reduction in the maximum temperature, as illustrated in Fig. 20. Thus when the hybrid circuit is designed, a device spacing of four device diameters or more will insure minimal thermal interaction between the devices. The devices can be placed closer if required, but the device temperatures will increase rapidly as the spacing is reduced.

## 7.2 *Isothermal Boundary Assumption Error*

A common assumption made in thermal analysis of hybrid substrates is that the interface between the substrate and heat sink (or case) is isothermal. This assumption is convenient since it decouples the analysis of the substrate from the heat sink. In the present model, a Biot number of infinity is equivalent to an isothermal interface. To compare the above example, where the coupling between the substrate and heat sink is

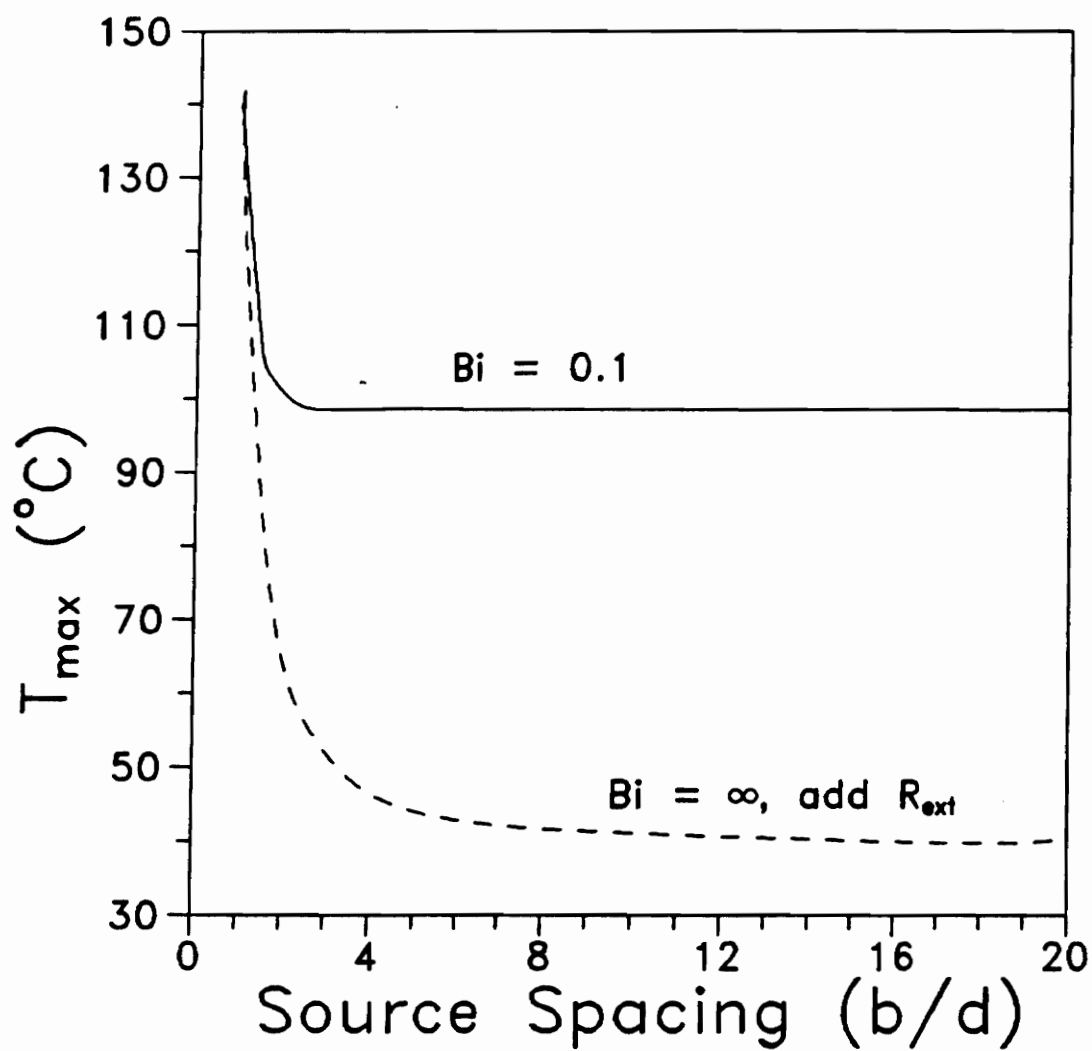


Figure 20. Maximum temperature examples for practical and isothermal boundary conditions

included, with a model where the substrate and heat sink are decoupled, we can calculate the temperature rise of the substrate alone ( $T_{\max} - T_{hs}$  in Fig. 13) using  $Bi = \infty$  and then add the temperature rise due to the heat sink external resistance ( $T_{hs} - T_0$  in Fig. 13) to that temperature. Thus, both methods can be compared on the basis of the total temperature rise,  $T_{\max} - T_0$ , with equivalent heat sink arrangements.

When the devices are adjacent to each other ( $B = 1$ ), the two methods give identical results. The Biot number has no effect on the heat flow path in the substrate since the flow is one-dimensional. As the spacing is increased to  $B = 4$ , the  $Bi = \infty$  results predict a maximum temperature of only  $47^\circ\text{C}$ , compared to a maximum temperature of  $99^\circ\text{C}$  when the substrate and heat sink are coupled, as shown in Fig. 13. The temperature then decreases gradually as  $B$  increases to 20. Clearly, the uncoupled method does not yield accurate results except when the heat flow is one-dimensional ( $B = 1$ ). For the  $Bi = \infty$  case, the temperature rise in the substrate alone is essentially independent of  $B$  and equal to  $10.1^\circ\text{C}$ . The gradual change with  $B$  shown in Fig. 15 is due to the changing heat sink temperature rise added to the temperature rise through the substrate to make a justifiable comparison with the  $Bi = 0.1$  case. The external resistance decreases as the square of  $B$  increases since more area of the heat sink is devoted to a single device (see Eq. 5.16).

## **8.0 Verification of Results**

Axisymmetric and experimental results were compared with three-dimensional results in order to verify the accuracy of the axisymmetric results. A three-dimensional analysis was performed using a computer program called TAMS (Ellison, 1978). Temperatures were measured experimentally using an Inframetrics 600 Thermal Imaging System. TAMS is deemed to be accurate and provides a test for determining the validity of the axisymmetric results presented in this work.

### ***8.1 Three-Dimensional Modeling***

A three-dimensional solution for the maximum temperature created by a device placed on a substrate was obtained using TAMS. TAMS yields a Fourier series solution for a

multi-layered system with lumped parameter thermal resistances on both the top and bottom surfaces. Each resistance terminates away from the substrate at a unique sink temperature. One or more sources may be placed on the substrate in a symmetrical or asymmetrical pattern.

To compare axisymmetric results with results from a full three-dimensional model, a square heat source was placed symmetrically at the center of a square substrate. TAMS results were obtained from this model, and the problem was then converted to an axisymmetric model and nondimensionalized. The maximum temperature values obtained from TAMS are compared with those obtained from the axisymmetric model for all geometries and boundary conditions used to tabulate axisymmetric results.

The three-dimensional model was also used to investigate the effect of eccentricity of heat sources. In two cases, substrates were fixed at sizes such that when the sources were placed symmetrically  $B = 20$  and  $B = 4$ . Tables 10 and 11 show the results from TAMS compared with axisymmetric results when the sources are placed symmetrically on the substrate and when they are brought progressively closer together. In these asymmetric cases, symmetry exists in the middle of the substrate between the sources, but heat can spread in the other directions without restraint. The axisymmetric results used for comparison derive  $B$  from source spacing only, and the extra substrate area is not considered. An example of a TAMS model with eccentrically spaced sources is shown in Fig. 21, and the axisymmetric model to which it is compared is shown in Fig. 22.



Table 11. Axisymmetric results vs. TAMS as two sources become asymmetric on a small substrate

BI = 0.01												BI = 1.0						BI = 100.0					
A = 0.1						A = 1.0						A = 0.1						A = 1.0					
B	$R_{tot,AXI}$ (K/W)		$R_{tot,TAM}$ (K/W)		% Error	$R_{tot,AXI}$ (K/W)		$R_{tot,TAM}$ (K/W)		% Error	$R_{tot,AXI}$ (K/W)		$R_{tot,TAM}$ (K/W)		% Error	$R_{tot,AXI}$ (K/W)		$R_{tot,TAM}$ (K/W)		% Error			
	$R_{tot,AXI}$ (K/W)	$R_{tot,TAM}$ (K/W)	$R_{tot,AXI}$ (K/W)	$R_{tot,TAM}$ (K/W)	% Error	$R_{tot,AXI}$ (K/W)	$R_{tot,TAM}$ (K/W)	$R_{tot,AXI}$ (K/W)	$R_{tot,TAM}$ (K/W)	% Error	$R_{tot,AXI}$ (K/W)	$R_{tot,TAM}$ (K/W)	$R_{tot,AXI}$ (K/W)	$R_{tot,TAM}$ (K/W)	% Error	$R_{tot,AXI}$ (K/W)	$R_{tot,TAM}$ (K/W)	$R_{tot,AXI}$ (K/W)	$R_{tot,TAM}$ (K/W)	% Error			
1.0	12.06	3.195	129.0	8.70	+1380	0.2546	0.2460	2.546	0.7536	+2.86	0.1288	0.1267	1.286	0.6184	+108								
1.6	5.533	2.736	50.45	8.612	+486	0.2464	0.2460	1.207	0.6786	+0.163	0.1205	0.1267	0.7144	0.5563	+27.7								
2.4	3.246	2.486	22.67	8.550	+165	0.2464	0.2460	0.7903	0.6416	+0.16	0.1265	0.1267	0.5686	0.5366	+8.15								
4.0	2.365	2.378	8.506	8.507	+0.02	0.2464	0.2460	0.6236	0.6270	+0.16	0.1265	0.1267	0.5322	0.5297	+0.472								



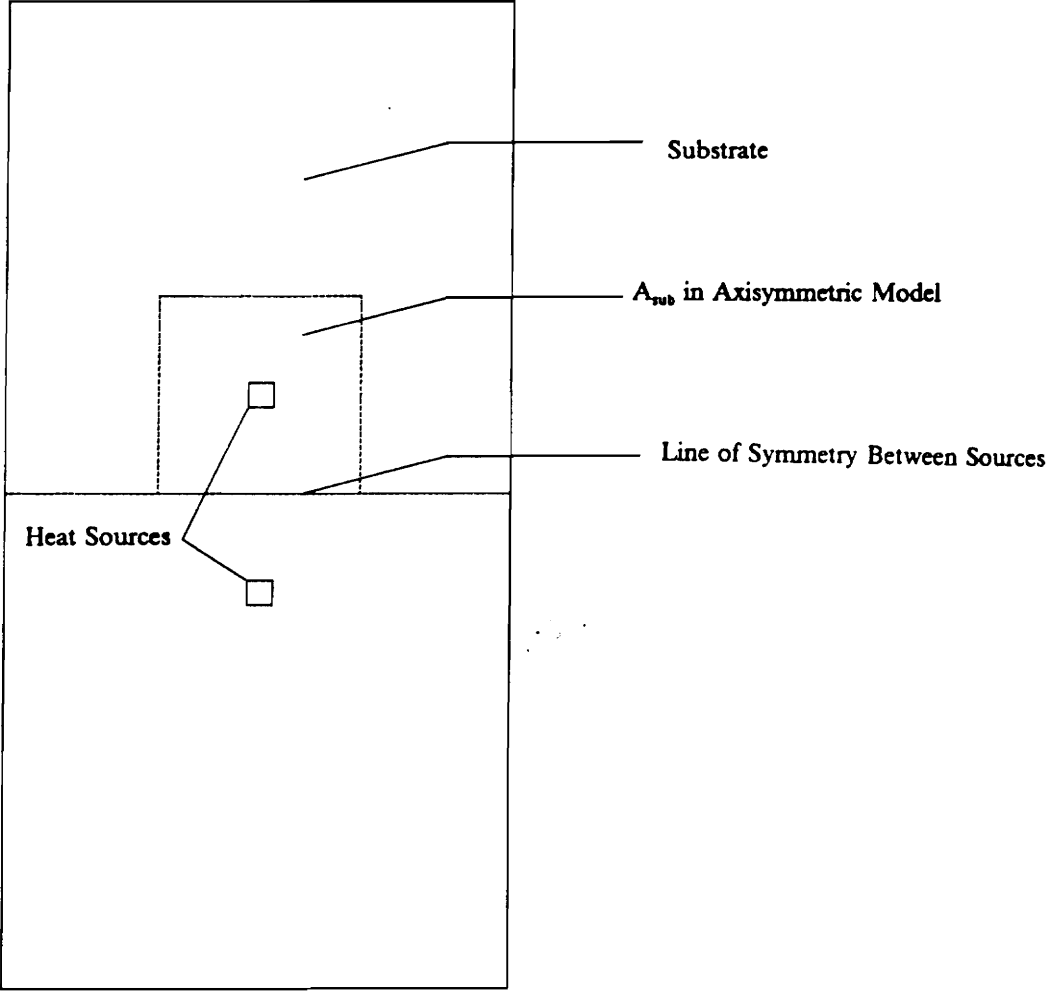
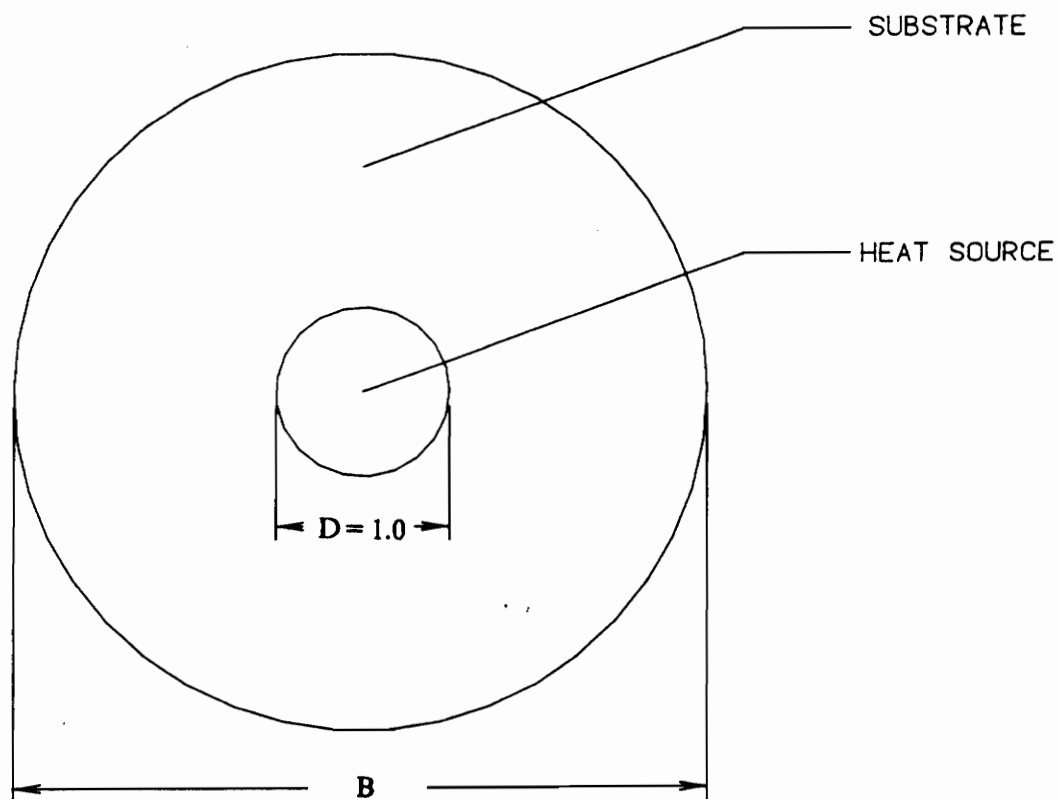


Figure 21. TAMS model of two sources placed eccentrically



**Figure 22.** Axisymmetric model of one source with reduced substrate area to compensate for eccentrically placed sources

Results are presented at two substrate thicknesses, three Biot numbers, and several source spacings. The model is developed as a three-dimensional problem, and the geometries and boundary conditions are input into TAMS. As with the symmetrical cases, the problem is converted into an axisymmetric model and nondimensionalized to compare with the axisymmetric results. Resistances are tabulated to make results independent of source power. A positive error means that the axisymmetric results predict a higher, or more conservative, maximum temperature.

When sources are symmetrically placed on a substrate, axisymmetric results predict maximum temperatures to within five percent of the temperatures predicted by TAMS in all cases, and usually within two percent. As eccentricity of the sources increases, axisymmetric results predict temperatures increasingly higher than those reported by TAMS. However, when  $A = 0.1$  and  $Bi$  is one or greater, axisymmetric results are accurate to within ten percent for even the most extremely eccentric sources. As the substrate thickness increases heat spreads radially more easily, making axisymmetric results less accurate when the sources are eccentric. Axisymmetric results usually predict conservative temperatures, are accurate when sources show symmetry, and, when  $A = 0.1$  and  $Bi$  is one or greater, are accurate when the sources are eccentric.

## 8.2 *Experimentation*

An Inframetrics 600 Thermal Imaging System was used to measure temperatures created by a resistor placed symmetrically on a substrate. Power dissipated by the resistor creates a flux which dissipates into the substrate. Negligible power is lost due to convection or radiation from the top of the resistor. By determining the maximum temperature created by the device, experimental results can be compared with results from TAMS to provide a measure of the accuracy of the experimental results.

The test substrate used to generate experimental results was 0.635 mm (0.025 in.) thick with an area of 1.82 cm<sup>2</sup>. One square device of area 0.0127 cm<sup>2</sup> was placed in the center of the substrate. Thus, in nondimensional parameters, A = 0.5 and B = 12. The electrical resistance through the device was 475 ohms, and 15 to 40 volts were placed incrementally across the circuit. The power dissipated by the device was calculated using the formula:

$$P = \frac{V^2}{R} \quad [8.1]$$

A thermal grease of known thermal conductivity was used to attach the substrate to a heat sink. The thermal resistance of the heat sink was estimated from a graph provided by the manufacturer.

A test apparatus was created to hold the heat sink, with the substrate bonded to it, vertically. Natural convection was the only means of heat dissipation from the heat

sink, which was held several inches over a table to eliminate any interference with convection by the table. Ambient temperature was measured to be 24°C. The thermal imaging system was held by a tripod, with lenses connected to focus on the substrate alone. Copper leads were connected to the substrate to make a solid connection to the power supply without interfering with the substrate or the thermal imaging system.

Emissivity of the resistor was measured by comparing it to a piece of black tape known to have an emissivity value of 0.95. The tape was placed below the resistor, and the tape and resistor were heated with a power stripper. The stripper blew hot air on the tape and resistor evenly so they would reach the same temperature. The emissivity of the tape was entered into the thermal imaging system menu, and its temperature was measured to be 82°C. Since the resistor was the same temperature as the tape, its emissivity could be found by adjusting the emissivity value in the thermal imaging system menu until the temperature of the resistor measured to be 82° also. The resistor emissivity value was measured to be 0.75, and this value was entered into the thermal imaging system menu.

Although the ambient air temperature was 24°C, the thermal imaging system was used to measure the surrounding surface temperature because the system measures infrared energy emitted by the surroundings, not the actual air temperature. A piece of aluminum foil, which has very high reflectivity, at room temperature was placed directly in front of the test substrate with the same orientation as the substrate to correctly measure energy that the substrate reflected from the surroundings. The thermal imaging system

measured the surrounding temperature to be 26°C , and this value was entered into the system menu.

Voltage output by the power supply was measured with a voltmeter to four significant digits and connected to the circuit. Once steady-state temperatures were reached, temperature measurements were made. Each maximum temperature created by the device was found by measuring temperatures at several points over the hottest area of the substrate for each voltage input level. The maximum temperature values measured by the system are presented in Table 12. The table lists the voltage input, the heat dissipated by the device, which is the same as the power calculated above, the heat flux,  $q_d''$ , which is the power per unit area, and  $T_{max,exp}$ , which is the maximum temperature measured by the thermal imaging system.

To help alleviate the problem of interpolating between Biot numbers, which is encountered when using the tabulated axisymmetric results, experimental results are compared to cases run using TAMS in Table 13. This comparison is more exact since the estimated thermal convective coefficient can be input into TAMS and the case can be solved quickly on a personal computer. Since axisymmetric results have been shown to compare closely with TAMS results at the same Biot number, the differences between experimental and TAMS results are considered to reflect the differences between experimental and axisymmetric results.

Results of a comparison between experimental maximum temperatures measured with a thermal imaging system and theoretical results from TAMS are presented in Table 13.

Table 12. Experimental results for temperatures created by one device placed symmetrically on a substrate

Voltage Input (V)	Power (W)	Device Flux $q_d''$ (kW/m <sup>2</sup> )	T <sub>max,exp</sub> (°C)
15.00	0.474	374	35
20.00	0.842	665	43
25.00	1.32	1040	55
30.00	1.89	1490	70
35.00	2.58	2040	90
40.00	3.37	2660	117

Table 13. Comparison of TAMS results to experimental results

Voltage Input (V)	$T_{max,TAM}$	$T_{max,exp}$	% Error
15.00	38.3	35	-37
20.00	49.4	43	-25
25.00	63.8	55	-22
30.00	80.9	70	-19
35.00	102	90	-15
40.00	125	117	-8.1



The temperature rise from ambient conditions created by the device is used to calculate the error in each case to eliminate the dependency of the result on the value of ambient temperature. Differences between the models are expected due to the nature of the experimental work. For example, though the only means of heat dissipation from the heat sink was intended to be natural convection, some air currents did exist in the room. These air currents may have induced some forced convection from the heat sink. Also, the resistor did not produce a uniform flux into the substrate due to the design of conductor leads used to power the resistor. Figure 23 shows the image produced by the thermal imaging system when twenty volts were placed across the resistor. The resistor and its leads are drawn over the image. Current entered the top left corner of the resistor and exited the bottom right corner. The white area represents the hottest points on the resistor. As the figure shows, the flux produced by the resistor is concentrated on the diagonal strip along which the current flowed. Therefore, it is concluded that some differences between experimental results and TAMS are accounted for by these inaccuracies in the testing procedure and the analysis of the system, and results of TAMS, and therefore axisymmetric results, compare reasonably well with experimental results.

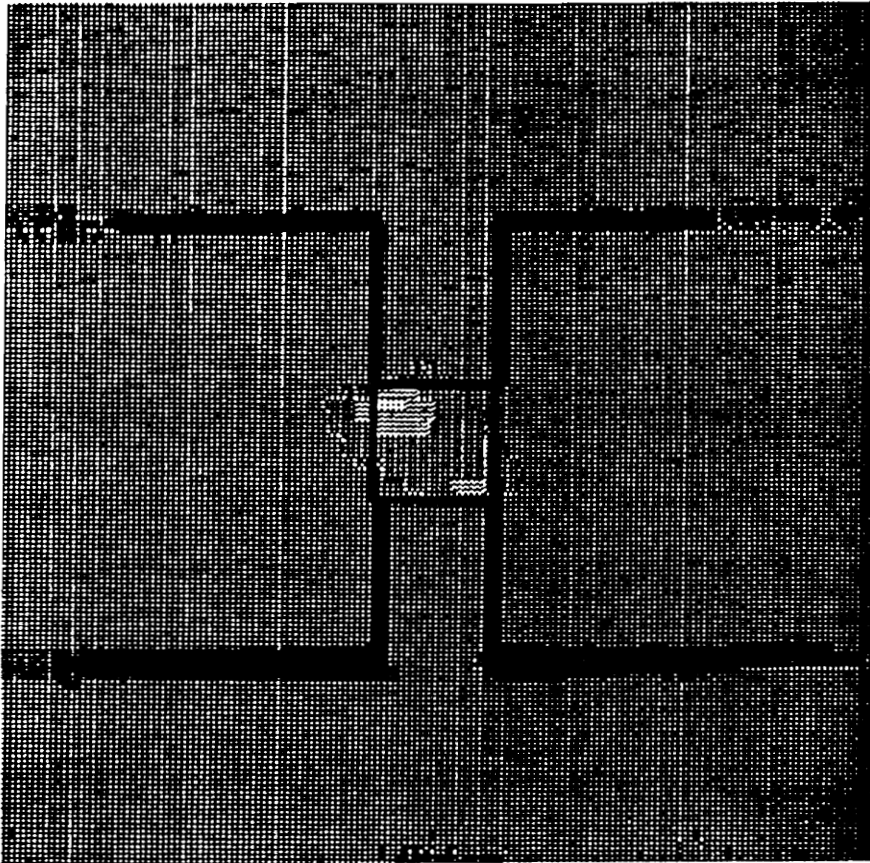


Figure 23. Image of a resistor and its leads produced by a thermal imaging system

## **9.0 Conclusions and Recommendations**

### ***9.1 Conclusions***

The results given in this paper are intended to aid in the design of hybrid power supplies. The interaction of sources on a substrate can be predicted to determine the temperature of the device. In addition to this, the concept of spreading resistance is examined. The heat flux path is shown to be a function of the geometry of the substrate as well as the external resistance below the substrate.

Several models are presented which predict maximum temperatures created by a device on a substrate. The one-dimensional model is simple, easy to understand, and provides a fast method of predicting maximum temperatures using only a calculator. However,

problems arise in deciding what heat spreading angle to use. The concept of a one-dimensional spread angle is encountered often in literature. Typically, a constant angle of heat propagation through a medium is assumed. The results of this work indicate that the path of heat propagation depends on the geometry of the medium as well as boundary conditions. In some cases, the spread angle concept is a good approximation. However, it is found in this work that the spread angle is not constant for all Biot numbers and geometries, making results of a one-dimensional model generally inaccurate.

Two two-dimensional models use finite difference codes to model a slice or slab of substrate with a heat source. Results yield the temperature distribution through the area of consideration. However, the path of heat propagation proves to be three-dimensional in nature since neither model predicts maximum temperatures accurately over a wide range of geometries or boundary conditions.

To accommodate the three-dimensional nature of the heat flow without having to perform a full three-dimensional analysis, an axisymmetric model is developed. The physical problem is then nondimensionalized, reducing the number of parameters from seven to three. The resulting governing equation is solved using the finite element method to obtain maximum temperature values. Nondimensional results for the maximum temperature and the resistance through the substrate are tabulated. By examining these results, certain trends are recognized.

- When the Biot number is small, the heat flux from the bottom of the substrate is approximately uniform.

- A Biot number approaching infinity is equivalent to an isothermal condition along the bottom of the substrate.
- When the nondimensional thickness is about half the width or greater the spreading resistance becomes independent of the Biot number.
- The maximum temperature is linear with  $A$  over the range of Biot numbers tested when  $B$  is constant and  $A$  is greater than two.
- For small Biot numbers at large widths, the maximum temperature, and therefore the total resistance, decreases with increasing thickness at first and then increases as thickness increases. Therefore, an optimal thickness exists to minimize the device temperature.
- When  $A$  is 0.1 and  $Bi$  is one or more, no interaction between devices occurs at  $B = 1.6$ . As thickness increases or Biot number decreases interaction between devices occurs at larger spacings. For example, when  $A$  is two and  $Bi$  is one or less, interaction between devices is not avoided until  $B$  is twenty.
- A truly semi-infinite condition exists when  $B$  is greater than twenty and  $A$  is greater than ten.

In order to verify the results obtained from the axisymmetric model, a three-dimensional analysis was performed using TAMS (Ellison, 1978). The maximum temperature values obtained from TAMS were compared with those obtained from the axisymmetric model for various geometries and boundary conditions. The maximum temperature values

calculated with TAMS differ from the axisymmetric temperatures by no more than five percent, with most being within two percent. The axisymmetric model proves to be very accurate when the actual heat source and substrate show symmetry.

In addition to verifying axisymmetric results with TAMS, temperatures were experimentally measured using an Inframetrics 600 Thermal Imaging System. Results of TAMS were compared to the experimental results since axisymmetric results are known to match temperatures predicted by TAMS. Several factors are known to limit the reliability of temperatures measured experimentally. Some forced convection was present and not accounted for, and the device did not create a uniform flux into the substrate. Considering these limitations, experimental results matched results from TAMS, and therefore axisymmetric results, adequately.

The results obtained from the axisymmetric model are intended to be used as a design tool for power hybrid microelectronics. After a preliminary design has been completed, including spacing of heat producing devices, geometry of the substrate, and heat sink conditions, thermal interaction can be evaluated without the necessity of a full three-dimensional model. In addition to this, existing circuits can be analyzed to predict reliability based on thermal interaction of devices within the design. Failures can be modeled to determine the degree to which high temperatures caused the breakdown. Therefore, although the results are intended to be used as a tool with which to design power hybrid microelectronic circuitry, they may also be used to examine current designs.

Some difficulties arise in modeling a physical problem using axisymmetric results. For example, determining an equivalent convective coefficient to represent all heat dissipating mechanisms below the substrate can be quite difficult. Heat sink manufacturers often provide data for the thermal resistance of their product, but the data may be hard to analyze and somewhat inaccurate. Another shortcoming of the axisymmetric results is interpolating between values tabulated since no correlating equations could be derived to represent the data. Often, slight changes in the Biot number, for example, can mean large changes in the maximum temperature predicted by the model. Finally, the axisymmetric model does not provide a method of accurately analyzing eccentrically placed devices on a substrate. Approximating the substrate area to represent  $b$  in such cases can lead to error in the results. Because of these problems encountered with the axisymmetric results, TAMS may be a better method of predicting thermal performance of hybrid microelectronics.

## ***9.2 Recommendations***

One recommendation for further research on this topic would be to develop correlating equations to describe nondimensional maximum temperatures which are currently tabulated. This would eliminate the need of interpolating between data points. Also, it would be beneficial to investigate maximum temperatures created by eccentrically placed heat sources on a substrate with an axisymmetric model. By altering the geometry parameters,  $A$  and  $B$ , the results presented in this work could describe the temperature rise created by eccentric sources.

Experimental work is time consuming, but results can have a large impact on theoretical analysis. Several configurations were to be manufactured and tested to verify results of the axisymmetric model. Unfortunately, problems arose in the fabrication of the test substrates and time constraints did not allow thorough testing to be done. With proper time and effort, more complete experimentation using the thermal imaging system would be an insightful addition to the theoretical results presented in this thesis.



## List of References

- Antonetti, V. W., and Yovanovich, M. M., 1984, "Thermal Contact Resistance in Microelectronic Equipment", *International Journal for Hybrid Microelectronics*, Vol. 7, No. 3, pp. 44-50.
- Beck, J. V., 1980, "Large Time Solutions for Temperatures in a Semi-Infinite Body with a Disk Heat Source", *International Journal of Heat and Mass Transfer*, Vol. 24, pp. 155-164.
- David, R. F., 1977, "Computerized Thermal Analysis of Hybrid Circuits", *IEEE Transactions on Parts, Hybrids, and Packaging*, CHMT, Vol. 13, No. 3, pp. 283-290.
- DeMey, G., and Demolder, S., 1987, "A Test Substrate for Thermal Analysis of Hybrid Circuits", *Hybrid Circuits*, No. 12, pp. 43-45.
- Ellison, G. N., 1978, "A Thermal Analysis Computer Program Applicable to a Variety of Microelectronic Devices", *Proceedings of the 1978 International Microelectronics Symposium*, pp. 332-339.
- Ellison, G. N., 1984, *Thermal Computations for Electronic Equipment*, Van Nostrand Reinhold Company, New York, pp. 322-327.
- Fast, D. W., Yovanovich, M. M., and Culham, J. R., 1987, "Correlation of Thermal Parameters Influencing the Differences Between One- and Two-Dimensional Con-

duction Within PCB's", *Proceedings of the International Symposium on Cooling Technology for Electronic Equipment*, pp. 423-430.

Ferraris, G. P., and Tudanca, M., 1979, "The Solution of Two-Dimensional Heat Conduction Problems to Predict Operating Temperature and Power Handling Capabilities of Hybrid Circuits", *Proceedings of the European Hybrid Microelectronics Conference*, pp. 61-74.

Frey, R. and Kane, M., 1985, "Temperature Effects Examined for Microwave Power-Transistor Performance and Thermal-Design Considerations", *Microwave Systems News & Communications Technology*, Vol. 15, No. 12, pp. 9-16.

Kadambi, V. and Abuaf, N., 1983, "Axisymmetric and Three-Dimensional Chip-Spreader Calculations", *AIChE Symposium Series*, Vol. 79, No. 225, pp. 130-139.

Kadambi, V. and Abuaf, N., 1985, "Numerical Thermal Analysis of Power Chip Packages", *Heat Transfer in Electrical Equipment*, ASME HTD, Vol. 48, pp. 77-84.

Kennedy, D. P., 1960, "Spreading Resistance in Cylindrical Semiconductor Devices", *Journal of Applied Physics*, Vol. 31, No. 8, pp. 1490-1497.

Negus, K. J. and Yovanovich, M. M., 1987, "Thermal Computations in a Semiconductor Die Using Surface Elements and Infinite Images", *Proceedings of the International Symposium on Cooling Technology for Electronic Equipment*, pp. 474-485.

Negus, K. J., Yovanovich, M. M., and Beck, J. V., 1989, "On the Nondimensionalization of Constriction Resistance for Semi-Infinite Heat Flux Tubes", *Journal of Heat Transfer*, Vol. 111, pp. 804-807.

Rottiers, L. and DeMay, G., 1988, "Simulation of Thermal Behaviour in Hybrid Circuits", *Intersociety Conference on Thermal Phenomena in the Fabrication and Operation of Electronic Components*, pp. 15-20.

Wehrhahn, E., 1985, "Temperature Distribution on Substrates of Hybrid Integrated Circuits", *Proceedings of the Fifth European Hybrid Microelectronics Conference*, pp. 288-295.

## Appendix A. Design Example Calculations

Consider a pattern of symmetrically spaced devices on a standard alumina substrate. The devices are square, with an area of  $3.17 \times 10^{-5} \text{ m}^2$ . Each device dissipates a flux of  $4 \times 10^5 \text{ W/m}^2$ , which corresponds to a total source power dissipation of 12.7 W. Symmetry between devices creates a square substrate area of  $5.07 \times 10^{-4} \text{ m}^2$  below each device. The substrate is 0.635 mm (0.025 in.) thick with a heat sink bonded to the bottom. All heat dissipating mechanisms below the substrate create an equivalent convective heat transfer coefficient of approximately  $4000 \text{ W/m}^2\text{-K}$  below the substrate. Heat dissipation from the top and sides of the substrate is negligible, and ambient air is  $30^\circ\text{C}$ .

To convert this model to an axisymmetric model, the device and substrate areas are held constant. The device and substrate below it are separated from other sources, with the original symmetry between devices creating insulated sides of the substrate. The heat source area is converted to a round region of area  $3.17 \times 10^{-5} \text{ m}^2$ , or source diameter of

$6.35 \times 10^{-3} \text{ m}$  . The substrate is converted to a cylinder of area  $5.07 \times 10^{-4} \text{ m}^2$ , or a diameter of  $2.54 \times 10^{-2} \text{ m}$ . The substrate thickness, source heat flux, and equivalent convection coefficient do not change in converting to an axisymmetric model. All dimensional quantities are listed below.

$$t = 6.35 \times 10^{-4} \text{ m} \quad [\text{A.1}]$$

$$k = 25 \text{ W/m-K} \quad [\text{A.2}]$$

$$d = 6.35 \times 10^{-3} \text{ m} \quad [\text{A.3}]$$

$$b = 2.54 \times 10^{-2} \text{ m} \quad [\text{A.4}]$$

$$h_{\text{eq}} = 4000 \text{ W/m}^2\text{-K} \quad [\text{A.5}]$$

$$T_0 = 30^\circ\text{C} \quad [\text{A.6}]$$

$$A_d = 3.17 \times 10^{-5} \text{ m}^2 \quad [\text{A.7}]$$

$$q_d'' = 4 \times 10^5 \text{ W/m}^2 \quad [\text{A.8}]$$

The model is nondimensionalized as follows.

$$K = 1.0 \quad [\text{A.9}]$$

$$D = 1.0 \quad [\text{A.10}]$$

$$A = \frac{t}{d} = 0.1 \quad [\text{A.11}]$$

$$B = \frac{b}{d} = 4.0 \quad [\text{A.12}]$$

$$\text{Bi} = \frac{ht}{k} = 0.1 \quad [\text{A.13}]$$

$$\theta_0 = 0 \quad [\text{A.14}]$$

Therefore, the three nondimensional parameters are:

$$A = 0.1 \quad [\text{A.15}]$$

$$B = 4.0 \quad [\text{A.16}]$$

$$\text{Bi} = 0.1 \quad [\text{A.17}]$$

From Tables 8 and 9,

$$\theta_{\max} = 0.6745 \quad [\text{A.18}]$$

$$\Phi_{\text{sp}} = 0.6906 \quad [\text{A.19}]$$

## ***A.1 Maximum Temperature Calculation***

The maximum temperature is found from the definition of  $\theta$ ,

$$\theta_{\max} = \frac{T_{\max} - T_0}{q_d'' d/k} \quad [\text{A.20}]$$

$$0.6745 = \frac{T_{\max} - 30^\circ\text{C}}{(4 \times 10^5 \text{ W/m}^2)(6.35 \times 10^{-3} \text{ m})/(25 \text{ W/m-K})} \quad [\text{A.21}]$$

$$T_{\max} = 98.5^\circ\text{C} \quad [\text{A.22}]$$

Therefore, the maximum temperature created by the device specified above on an alumina substrate with the specified device spacing is predicted to be  $98.5^\circ\text{C}$ .

## ***A.2 Isothermal Boundary Assumption Error***

If the temperature along the bottom of the substrate is assumed to be constant, the equivalent Biot number is infinity. Therefore, the three parameters are:

$$A = 0.1 \quad [\text{A.23}]$$

$$B = 4.0 \quad [\text{A.24}]$$

$$Bi = \infty \quad [A.25]$$

From tables 8 and 9,

$$\theta_{\max} = 0.09988 \quad [A.26]$$

$$\Phi_{sp} = 0.1127 \quad [A.27]$$

Again, the definition of theta is used, but this time to calculate the temperature rise through just the substrate.

$$0.09988 = \frac{T_{\max} - T_{hs}}{q_d'' d/k} \quad [A.28]$$

$$T_{\max} - T_{hs} = 10.1^{\circ}\text{C} \quad [A.29]$$

The temperature rise through the heat sink,  $T_{hs} - T_0$ , is zero when the Biot number is infinity. However, the temperature rise through the heat sink from the  $Bi = 0.1$  case is used. Adding the temperature rise through the substrate to the temperature rise through the heat sink yields the total temperature rise predicted when the bottom of the substrate is assumed to be isothermal. From the maximum temperature calculations, the temperature rise through the heat sink is obtained from the following dimensional formula:

$$Q = q_d'' \frac{\pi d^2}{4} = \frac{T_{hs} - T_0}{R_{ext}} \quad [A.30]$$

where

$$Q = (4 \times 10^5 \text{ W/m}^2) \frac{\pi}{4} (6.35 \times 10^{-3} \text{ m})^2 = 12.7 \text{ W} \quad [\text{A.31}]$$

$$R_{\text{ext}} = \frac{1}{k\sqrt{A_d}} \frac{1}{\sqrt{\pi/4}} \frac{A}{B^2 \text{Bi}} = 0.501 \text{ K/W} \quad [\text{A.32}]$$

Therefore,

$$T_{\text{hs}} - T_0 = 6.35^\circ\text{C} \quad [\text{A.32}]$$

The total temperature rise,  $(T_{\text{max}} - T_{\text{hs}}) + (T_{\text{hs}} - T_0)$ , is  $16.5^\circ\text{C}$ . Adding the ambient temperature to get  $T_{\text{max}}$ ,

$$T_{\text{max}} = 46.5^\circ\text{C} \quad [\text{A.33}]$$

Thus, under the same conditions as originally specified, except the assumption of an isothermal boundary at the bottom of the substrate, the maximum temperature is  $46.5^\circ\text{C}$ . This is a 52.8% difference from the maximum temperature calculated above. Therefore, the assumption of a constant temperature at the bottom of the substrate is invalid.



## Vita

Herbert H. Eades, III was born on September 19, 1967 in Richmond, Virginia. He was graduated from J. R. Tucker High School in June, 1985. He attended Virginia Polytechnic Institute and State University, where he was an active German Club memeber and served as President of the Virginia Tech A.S.M.E. Student Section. In May, 1989, he was graduated from Virginia Tech with a Bachelor of Science in Mechanical Engineering. The same month, he enrolled in the Graduate School of Virginia Tech. In July, 1990, he was graduated with a Master of Science in Mechanical Engineering. Upon leaving Virginia Tech, he began work for Westinghouse Electric Corporation as a Nuclear Engineer training at the Naval Training Center in Orlando, Florida.